

# 1 **Assessing the ammonium nitrate formation regime in the** 2 **Paris megacity and its representation in the CHIMERE** 3 **model**

4

5 **H. Petetin<sup>1,\*</sup>, J. Sciare<sup>2,3</sup>, M. Bressi<sup>2</sup>, A. Rosso<sup>4</sup>, O. Sanchez<sup>4</sup>, R. Sarda-**  
6 **Estève<sup>2</sup>, J.-E. Petit<sup>2,\*\*</sup>, and M. Beekmann<sup>1</sup>**

7 (1) {LISA/IPSL, Laboratoire Inter-universitaire des Systèmes Atmosphériques, UMR CNRS 7583,  
8 Université Paris Est Créteil (UPEC) and Université Paris Diderot (UPD), France}

9 (2) {LSCE, Laboratoire des Sciences du Climat et de l'Environnement, CNRS-CEA-UVSQ, Gif-  
10 sur-Yvette, France}

11 (3) {Energy Environment Water Research Center (EEWRC), The Cyprus Institute, Nicosia,  
12 Cyprus}

13 (4) {AIRPARIF, Agence de surveillance de la qualité de l'air, Paris, France}

14 \* now at: Laboratoire d'Aérodynamique, Université Paul Sabatier and CNRS, Toulouse, France

15 \*\* now at: Air Lorraine, Villers-les-Nancy, France

16 Correspondence to: H. Petetin ([hervepetetin@gmail.com](mailto:hervepetetin@gmail.com))

17

## 18 **Abstract**

19 Secondary inorganic compounds represent a major fraction of fine aerosol in the Paris megacity.  
20 The thermodynamics behind their formation is now relatively well constrained, but due to sparse  
21 direct measurements of their precursors (in particular  $\text{NH}_3$  and  $\text{HNO}_3$ ), uncertainties remain on their  
22 concentrations and variability as well as the formation regime of ammonium nitrate (in terms of  
23 limited species, among  $\text{NH}_3$  and  $\text{HNO}_3$ ) in urban environments such as Paris. This study presents  
24 the first urban background measurements of both inorganic aerosol compounds and their gaseous  
25 precursors during several months within the city of Paris. Intense agriculture-related  $\text{NH}_3$  episodes  
26 are observed in spring/summer while  $\text{HNO}_3$  concentrations remain relatively low, even during  
27 summer, which leads to a  $\text{NH}_3$ -rich regime in Paris. The local formation of ammonium nitrate  
28 within the city appears low, despite high  $\text{NO}_x$  emissions. The dataset also allows evaluating the  
29 CHIMERE chemistry-transport model (CTM). Interestingly, the rather good results obtained on  
30 ammonium nitrates hide significant errors on gaseous precursors (e.g. mean bias of -75 and +195%  
31 for  $\text{NH}_3$  and  $\text{HNO}_3$ , respectively). This leads to a mis-representation of the nitrate formation regime

1 through a highly underestimated Gas Ratio metric (introduced by Ansari and Pandis (1998)) and a  
2 much higher sensitivity of nitrate concentrations to ammonia changes. Several uncertainty sources  
3 are investigated, pointing out the importance of better assessing both  $\text{NH}_3$  agricultural emissions  
4 and OH concentrations in the future. These results finally remind the caution required in the use of  
5 CTMs for emission scenario analysis, highlighting the importance of prior diagnostic and dynamic  
6 evaluations.

## 7 **1 Introduction**

8 Atmospheric particulate matter (PM) consists in a complex mixture of various organic and  
9 inorganic compounds known for causing serious adverse effects on human health (Chow, 2006;  
10 Pope et al., 2009), in particular close to primary sources in urban environments. Through acidic  
11 deposition, it also affects both ecosystems (Camargo and Alonso, 2006; Grantz et al., 2003) and  
12 monuments (Lombardo et al., 2013). It plays a crucial but still uncertain role in climate change  
13 through interactions with radiation and clouds formation, leading at a global scale to a radiative  
14 forcing estimated between  $-1.9$  and  $-0.1 \text{ W.m}^{-2}$  at a 95% confidence interval (IPCC, 2013). Among  
15 the various chemical constituents of PM, nitrate ( $\text{NO}_3^-$ ) contributes significantly in the form of  
16 semi-volatile ammonium nitrate to the fine (PM with aerodynamic diameter below  $2.5 \mu\text{m}$ ) and  
17 coarse (aerodynamic diameter between  $2.5$  and  $10 \mu\text{m}$ ) aerosol modes, with mean contributions in  
18 Europe around 6-16 and 6-20%, respectively (Putaud et al., 2010). Several studies have reported  
19 increasing ammonium nitrate relative contributions with increasing PM mass concentrations at  
20 urban sites, thus underlying their importance in exceedances of European PM standards (Putaud et  
21 al., 2010; Yin and Harrison, 2008). Such a pattern has been evidenced for the city of Paris by Sciare  
22 et al. (2010), Bressi et al. (2013) and Petit et al. (2015) and clearly points to the need for a better  
23 understanding of the processes controlling the formation of ammonium nitrate.

24 Ammonium nitrate formation primarily results from both the formation of nitric acid ( $\text{HNO}_3$ ) and  
25 the emission of ammonia ( $\text{NH}_3$ ) under favorable thermodynamic conditions.  $\text{NO}_2$  is converted into  
26  $\text{HNO}_3$  through oxidation by the OH radical (homogeneous direct pathway) or ozone (through the  
27 formation of several intermediate compounds, including nitrate radical  $\text{NO}_3$  and nitrogen pentoxide  
28  $\text{N}_2\text{O}_5$ ; heterogeneous indirect pathway) (Seinfeld and Pandis, 2006). The first pathway is expected  
29 to dominate during daytime, when OH concentrations are the highest (Matsumoto and Tanaka,  
30 1996). Conversely, due to the very short lifetime of the  $\text{NO}_3$  radical in the presence of solar  
31 irradiation (Vrekoussis et al., 2004), the second pathway mainly acts during nighttime, favored by  
32 decreasing temperature and increasing relative humidity (RH), or during fog events ((Platt et al.,  
33 1981); Dall'Osto et al., 2009; Healy et al., 2012). Additionally, some  $\text{HNO}_3$  may also be directly  
34 emitted by both anthropogenic and natural (e.g. volcanoes, Mather et al., 2004) sources.  $\text{NH}_3$  is  
35 mainly emitted by agricultural activities (at 93% in France, CITEPA (2013)), with several other

1 minor sources including industry, traffic (e.g. Kean et al., 2009; Bishop et al., 2010; Carslaw and  
2 Rhys-Tyler, 2013; Yao et al., 2013) or sewage disposal (Sutton et al., 2000). In the presence of NH<sub>3</sub>  
3 available after the neutralization of sulfate, a thermodynamic equilibrium is reached between HNO<sub>3</sub>  
4 and NH<sub>3</sub>, which potentially leads to the formation of NH<sub>4</sub>NO<sub>3</sub> in the aqueous or solid phase,  
5 depending on temperature, RH and sulfate concentrations (Ansari and Pandis, 1998; Mozurkewich,  
6 1993). In marine environments, HNO<sub>3</sub> may also adsorb onto NaCl salts and react to form sodium  
7 nitrate (NaNO<sub>3</sub>) in the coarse fraction (Harrison and Pio, 1983; Ottley and Harrison, 1992). The  
8 relationship between nitrate aerosols and its gaseous precursors is thus highly non-linear (Ansari  
9 and Pandis, 1998), and the calculation of nitrate concentrations requires the use of thermodynamic  
10 models able to determine the partitioning of inorganic compounds between the gaseous and aerosol  
11 (aqueous or solid) phases depending on the temperature and RH conditions (see Fountoukis and  
12 Nenes, 2007 for a review).

13 Considering the high contribution of nitrate to fine particulate pollution, both the identification of  
14 the limited species (among NH<sub>3</sub> and HNO<sub>3</sub>) in the formation of NH<sub>4</sub>NO<sub>3</sub> and the quantification of  
15 the PM response to a given emission reduction of either precursor are crucial information for air  
16 quality management authorities in charge of designing efficient PM control strategies. Various  
17 approaches have been proposed in the literature to investigate these points. Chemistry-transport  
18 models (CTMs) simulations and emission reduction scenarios remain the easiest way to provide a  
19 first guess of the limited species and PM response to emission changes. Over Europe, several  
20 studies with different CTMs have simulated a HNO<sub>3</sub>-limited regime (Sartelet et al., 2007 and Kim  
21 et al., 2011 with the POLYPHEMUS model; Hamaoui-Laguel et al., 2014 with the CHIMERE  
22 model; Pay et al., 2012 with the CALIOPE-EU modelling system). However, such an approach  
23 relies on the good performance of CTMs that still suffer from various uncertainties, in particular in  
24 their input data (e.g. emission inventories). In respect to these perspectives, comparisons with field  
25 observations are highly valuable for evaluating model outputs. When measurements of total nitrate  
26 (TNO<sub>3</sub>=HNO<sub>3(g)</sub>+NO<sub>3</sub><sup>-</sup>), total ammonia (TNH<sub>3</sub>=NH<sub>3(g)</sub>+NH<sub>4</sub><sup>+</sup>) and total sulfate  
27 (TS=H<sub>2</sub>SO<sub>4(g)</sub>+HSO<sub>4</sub><sup>-</sup>+SO<sub>4</sub><sup>2-</sup>) are available, it is possible to diagnose which precursor is limiting  
28 nitrate formation. A first approach relies on the use of the gas ratio (GR) defined as the ratio of free  
29 ammonia after sulfate neutralization (FNH<sub>x</sub>(μmol m<sup>-3</sup>) =NH<sub>3</sub>+NH<sub>4</sub><sup>+</sup>-2xSO<sub>4</sub><sup>2-</sup>) over total nitrate  
30 (TNO<sub>3</sub>(μmol m<sup>-3</sup>)=HNO<sub>3</sub>+NO<sub>3</sub><sup>-</sup>) (Ansari and Pandis, 1998). GR values above unity indicate a  
31 regime mainly limited by HNO<sub>3</sub> (e.g. NH<sub>3</sub>-rich regime) in which there is enough NH<sub>3</sub> to neutralize  
32 both sulfate and nitrate. Conversely, GRs between zero and one indicate that there is enough NH<sub>3</sub> to  
33 neutralize sulfate but not nitrate, while negative GRs correspond to a NH<sub>3</sub>-poor regime in which  
34 NH<sub>3</sub> amounts are insufficient to even neutralize sulfate. Based on the *European Monitoring and*  
35 *Evaluation Program* (EMEP) regional background observations, Pay et al. (2012) obtained GRs  
36 above unity (i.e. a HNO<sub>3</sub>-limited regime) over continental Europe, in reasonable agreement with the

1 CALIOPE model. Conversely, a  $\text{NH}_3$ -limited regime was found over ocean and closer to coasts in  
2 some countries (e.g. Spain, England, countries around Baltic Sea) due to ship emissions of  $\text{SO}_2$  and  
3  $\text{NO}_x$  and low  $\text{NH}_3$  over marine regions. However, the determination of the limited compound based  
4 on GR is valid only under the assumption of a complete transfer (of the limited species) in the  
5 aerosol phase (i.e. at low temperature and high RH). Under ambient conditions favoring a  
6 partitioning between both phases, both  $\text{NH}_3$  and  $\text{HNO}_3$  exist in the gas phase and the nitrate  
7 formation may be sensitive to changes in one or the other precursor. A more realistic assessment of  
8 the nitrate formation regime can be obtained by performing sensitivity tests on thermodynamic  
9 models fed by field measurements (concentrations, temperature and RH). Such an approach allows  
10 quantifying the PM response to total reservoir (either  $\text{TNH}_3$ ,  $\text{TNO}_3$  or TS) concentrations reductions  
11 (Ansari and Pandis, 1998 and Takahama et al., 2004 with the GFEMN model; Blanchard and Hidy,  
12 2003 with the SCAPE2 model). These studies rely on the hypothesis that the concentration  
13 reduction of one specific compound does not affect the others, which is not true due to lifetime  
14 differences between gas and aerosol phases induced by contrasted deposition rates; for instance, a  
15 reduction of sulfate increases the amount of  $\text{FNH}_x$  available for the formation of nitrate that deposit  
16 less than  $\text{HNO}_3$  (Davidson and Wu, 1990), which finally increases the  $\text{TNO}_3$  reservoir. These  
17 difficulties may be overcome through the combined use of observations and deposition  
18 parameterizations in observation-based box models (Vayenas et al., 2005). As these models cannot  
19 integrate the whole complexity at stake in the atmosphere, CTMs are still needed to assess the  
20 nitrate formation regime and the PM response to precursors changes, but require in turn to be  
21 validated by experimental data.

22 This paper aims at investigating the variability and sources of both  $\text{HNO}_3$  and  $\text{NH}_3$ , and the  
23 associated  $\text{NH}_4\text{NO}_3$  formation regime in the Paris megacity, as well as the ability of the CHIMERE  
24 regional CTM to reproduce it. To this end, an important experimental effort, in the framework of  
25 the PARTICULES and FRANCIPOL projects, has recently made available a large database of fine  
26 aerosol chemical compounds (e.g. nitrate, ammonium, sulfate) and inorganic gaseous precursors  
27 (e.g.  $\text{HNO}_3$ ,  $\text{NH}_3$ ) in the region of Paris. To our knowledge, this is the first time that simultaneous  
28 measurements of inorganic compounds in both gaseous and aerosol phases, covering most seasons  
29 are performed in France. Experimental aspects are described in Sect. 2. The CHIMERE model and  
30 its setup is then introduced in Sect. 3. Results are shown and discussed in Sect. 4, and overall  
31 conclusions are given in Sect. 5.

## 32 **2 Experimental**

### 33 **2.1 Fine aerosols measurements**

34 As part of the AIRPARIF-LSCE “PARTICULES” project (Airparif, 2011, 2012), fine aerosol  
35 particles ( $\text{PM}_{2.5}$ ) were collected every day during 24 h (from 00:00 to 23:59 LT) during one year

1 (from 11 September 2009 to 10 September 2010) using two collocated Leckel low volume samplers  
2 (SEQ47/50) running at  $2.3 \text{ m}^3 \text{ h}^{-1}$ . One Leckel sampler was equipped with quartz filters (QMA,  
3 Whatman, 47 mm diameter) for carbon analyses, the second with Teflon filters (PTFE, Pall, 47 mm  
4 diameter,  $2.0 \text{ }\mu\text{m}$  porosity) for gravimetric and ion measurements (including  $\text{NH}_4^+$ ,  $\text{NO}_3^-$ ,  $\text{SO}_4^{2-}$ ).  
5 Six sampling sites were implemented, covering the region of Paris. Only the results for the  
6 background station located in the city center of Paris (4<sup>th</sup> district,  $48^\circ 50' 56'' \text{N}$ ,  $02^\circ 21' 55'' \text{E}$ , 20 m  
7 above ground level, a.g.l.) will be presented here. More information on the experimental setup and  
8 quality control of the datasets is available in Bressi et al. (2013). Note that filter measurements are  
9 subject to artefacts, through the evaporation and/or the adsorption of semi-volatile compounds  
10 (Pang et al., 2002), and thus mostly affect ammonium nitrate and organic matter concentrations.  
11 Daily chemical mass closure studies and comparisons with on-line artefact-free measurements were  
12 performed for that purpose and showed that filter sampling was quite systematically missing about  
13 20% of  $\text{PM}_{2.5}$  (15% of fine nitrate; Bressi et al., 2013).

14

## 15 **2.2 Gaseous precursors measurements**

16 As part of the PRIMEQUAL (*Programme de Recherche Interorganisme pour une MEilleure*  
17 *QQualité de l'Air à l'échelle Locale*) « FRANCIPOL » project, gaseous precursors ( $\text{NH}_3$ ,  $\text{HNO}_3$ ,  
18  $\text{SO}_2$ ) were monitored in near real-time on the roof platform (14 m a.g.l.) at the Laboratoire  
19 d'Hygiène de la Ville de Paris (LHVP) in the heart of Paris (13th district). Gas-phase  $\text{NH}_3$   
20 measurements were obtained for a 10-month period (May 2010 – February 2011) every 5 min using  
21 an AiRRmonia monitor (Mechatronics Instruments BV, The Netherland). The March/April periods  
22 (2010 and 2011) were missing due to technical problems with the instrument. Based on  
23 conductivity detection of  $\text{NH}_4^+$ , gaseous  $\text{NH}_3$  were sampled at  $1 \text{ L min}^{-1}$  using a 1-m long Teflon  
24 (1/2 inch diameter) sampling line. It was then collected through a sampling block equipped with an  
25  $\text{NH}_3$ -permeable membrane; a demineralized water counter-flow allows  $\text{NH}_3$  to solubilize in  $\text{NH}_4^+$ .  
26 A second purification step was applied by adding 0.5 mM sodium hydroxide, leading to the  
27 detection of  $\text{NH}_4^+$  in the detector block. The instrument was calibrated regularly (twice per months)  
28 using 0 ppb and 500 ppb  $\text{NH}_4^+$  aqueous solution (NIST standards). Two sets of sampling syringes  
29 ensure a constant flow throughout the instrument, but also create a temporal shift, ranging from 10  
30 to 40 min for different studies (Erisman et al., 2001; Cowen et al., 2004; Zechmeister-Boltenstern,  
31 2010; von Brobrutzki et al., 2010). We have taken here a constant value of 30 min for this delay in  
32 time response. Detection limit and precision of the instrument are typically  $0.1 \text{ }\mu\text{g m}^{-3}$  and 3 to  
33 10%, respectively (Erisman et al., 2001; Norman et al., 2009). More than 62,000 valid data points  
34 of  $\text{NH}_3$  - covering 217 days - were obtained with the AiRRmonia instrument and used for this study.

1 HNO<sub>3</sub> and SO<sub>2</sub> were analyzed continuously for an 11-month period (March 2010 – January 2011)  
2 using a Wet Annular Denuder (WAD) similar to the one reported in details by Trebs et al. (2004)  
3 and coupled with Ion Chromatography (IC). Briefly, whole air was sampled at ~10 L min<sup>-1</sup> in the  
4 WAD. This air flowrate – slightly below the 17 L min<sup>-1</sup> usually set – was taken to ensure a laminar  
5 flow and minimize particle losses onto the walls of the WAD and thus minimize possible artefacts  
6 in our IC (anion) measurements that could raise from inorganic salts present in the particulate  
7 phase. Following the recommendations by Neuman et al. (1999), our sampling line were made of  
8 plastic (PE, 1/2 inch diameter, John Guest, USA) and reduced to 1 m in order to keep a residence  
9 time of sampled air below 1s preventing formation/losses of NH<sub>4</sub>NO<sub>3</sub> (Dlugi 1993). 18.2 MΩ water  
10 was used to rinse the WAD at a flowrate of ~ 0.40 ml min<sup>-1</sup> and feed the IC with the solubilized  
11 acid gases. The IC (ICS2000, Dionex) configuration setup is similar to the one reported by (Sciare  
12 et al., 2011). Time resolution (chromatogram) was typically 15 min for the major gaseous acidic  
13 species (HCOOH, CH<sub>3</sub>COOH, HCl, HONO, HNO<sub>3</sub>, SO<sub>2</sub>). Oxidation of SO<sub>2</sub> into SO<sub>4</sub><sup>2-</sup> in the liquid  
14 flow downstream of the WAD was performed by solubilization of ambient oxidants such as H<sub>2</sub>O<sub>2</sub>.  
15 Based on these settings, detection limit for acidic gases was typically below 0.1 μg m<sup>-3</sup>.  
16 Uncertainties in ambient concentrations of acidic gases depend on air and liquid flowrates  
17 (controlled on a weekly basis) as well as the IC calibration (performed every 2 months). Overall  
18 standard deviations (1 σ) of 6%, 15% and 10% were calculated for these 3 parameters (air flowrate,  
19 liquid flowrate, IC calibration), respectively, leading a total uncertainty of about 20% for the WAD-  
20 IC measurements.

21 This WAD technique has been successfully intercompared with off-line techniques in (Trebs et al.,  
22 2008). Further comparison of the WAD-IC technique was performed during our study with a  
23 commercially available SO<sub>2</sub> analyzer (AFM22, Environnement S.A.) for a period of 3 months.  
24 Despite the poor detection limit (1 ppb = 2.43 μg m<sup>-3</sup>) of the commercially available instrument and  
25 the low ambient concentrations recorded at our station with SO<sub>2</sub> monthly means ranging from 0.76  
26 to 3.03 μg m<sup>-3</sup> measured with our WAD-IC instrument, quite consistent results were obtained from  
27 this intercomparison (slope of 0.73 and r<sup>2</sup>=0.56 for n=1671 hourly averaged data points). More than  
28 24,000 valid data points of SO<sub>2</sub> and HNO<sub>3</sub> - covering 253 days - were obtained with the WAD-IC  
29 instrument and used for this study.

### 30 **2.3 Meteorological parameters measurement**

31 Beside chemical compounds, traditional meteorological parameters — temperature, wind speed and  
32 direction, RH — are also measured at the MONTSOURIS station (2.337°E, 48.822°N) in Paris,  
33 close to the LHVP site (~ 2 km). In addition, boundary layer height (BLH) estimations are retrieved  
34 from an aerosol lidar at the SIRTAs (*Site Instrumental de Recherche par Télédétection*  
35 *Atmosphérique*) site (48.712°N, 2.208°E) (Haeffelin et al., 2012).

1  
2 This paper will focus on measurements performed from the 1 April to 31 December 2010. Note  
3 that all the measurements described in previous sections come from different campaigns and  
4 measurement periods that do not entirely overlap. Measurements of secondary inorganic aerosols  
5 ( $\text{NH}_4^+$ ,  $\text{NO}_3^-$ ,  $\text{SO}_4^{2-}$ ) are available daily between the 1 April and the 10 September 2010.  $\text{NH}_3$   
6 ( $\text{HNO}_3$ ) observations are available hourly from the 20 May (1 April) to the 31 December 2010.  
7

## 8 **2.4 Representativeness and datasets combination**

9 The purpose of this study is to investigate the relation of  $\text{NH}_4\text{NO}_3$  with its gaseous precursors,  
10 which ideally requires co-located measurements of all compounds in both phases. This was not the  
11 initial purpose of PARTICULES and FRANCIPOL projects, and thus, no such co-located  
12 observations are available in Paris. However, we argue here that the two datasets (inorganic  
13 aerosols measured in the 4<sup>th</sup> district of Paris, and gaseous precursors measured in the 13<sup>th</sup> district)  
14 can be reasonably considered as co-located and representative of the urban background of at least  
15 the southern half of the Paris city.

16 Several elements support this hypothesis. First, both sites are only ~3 km away from each other.  
17 Second, both sites are located on the rooftop of rather high buildings (20 and 14 m a.g.l.), thus quite  
18 far from direct influence of local pollution sources (e.g. traffic) and at a height where the venting of  
19 pollution is favored by the absence of obstacles and likely stronger winds (compared to the street  
20 level). The height of the LHVP roof site is slightly lower compared to the other site, but the  
21 building is located in a public garden, which further limits the possibility of local contamination by  
22 surrounding pollution sources. Third, based on the  $\text{PM}_{2.5}$  chemical speciation measurements  
23 performed both inside Paris and at several rural sites all around the Paris region during a whole  
24 year, the PARTICULES project has shown that secondary inorganic aerosols in the Paris urban  
25 background are mostly imported from outside the city (Petetin et al., 2014). At the annual scale, the  
26 contribution of imports was estimated to be 78% for nitrate, 90% for ammonium and 98% for  
27 sulfates (see Table 6 in Petetin et al., 2014). This is mostly explained by (i) the presence of strong  
28 pollution reservoirs in Europe (e.g. Benelux, eastern Europe) from where large plumes can be  
29 advected toward Paris under certain meteorological conditions, (ii) the time necessary for the  
30 formation of inorganic aerosols (including the oxidation of  $\text{NO}_x$  and  $\text{SO}_2$ ) is too low to allow a  
31 strong local production that thus preferentially occurs downwind in the Paris plume, as observed  
32 during the MEGAPOLI campaign (Freney et al., 2014), and (iii) the limited occurrence of stagnant  
33 conditions in Paris (that would allow enough time for gaseous precursors to produce inorganic  
34 aerosols). The high contribution of imported pollution is confirmed by the comparison of daily  
35 inorganic aerosol concentrations between the 4<sup>th</sup> district site and a traffic site located along the Paris

1 ring 8 km westward, that shows a very good correlation for all inorganic aerosols during the whole  
2 year (ammonium:  $y=0.95x+0.02$ ,  $R=0.97$ ,  $N=325$  ; nitrate:  $y=0.99x-0.09$ ,  $R=0.98$ ,  $N=325$  ; sulfate:  
3  $y=1.04x+0.01$ ,  $R=0.98$ ,  $N=325$ ). Thus, concerning secondary inorganic aerosols, the urban  
4 background can be considered as rather homogeneous at the scale of the whole Paris agglomeration.  
5 And observations in the 4<sup>th</sup> district of Paris can be reasonably combined to gaseous precursors  
6 observations at the other site.

7 In terms of spatial representativeness for  $\text{HNO}_3$  and  $\text{NH}_3$ , no other measurements are available to  
8 quantitatively assess the homogeneity of their urban background. In particular, some  $\text{NO}_x$  emitted  
9 within the center of the city may be already converted into  $\text{HNO}_3$  at the borders of the Paris  
10 agglomeration, leading to higher concentrations compared to the center of Paris. Thus, one cannot a  
11 priori consider these measurements representative of the urban background at the scale of the whole  
12 Paris agglomeration. However, as we already discussed, considering the morphology and the  
13 geographical location of the LHVP site, one can reasonably consider that it is representative of the  
14 urban background of at least the southern half of Paris city.

15

### 16 **3 Model setup and input data**

#### 17 **3.1 CHIMERE model description**

18 Simulations are performed using the CHIMERE CTM (Schmidt and Derognat, 2001; Bessagnet et  
19 al., 2009; Menut et al., 2013) ([www.lmd.polytechnique.fr/chimere](http://www.lmd.polytechnique.fr/chimere)) which is designed to provide  
20 short-term predictions of ozone and aerosols, as well as to help emissions mitigation assessment  
21 through emission reduction scenarios. It is used both in research activities and operational air  
22 quality monitoring and forecasting at the local, national and European scale (ESMERALDA over  
23 the northern part of France; PREVAIR service, [www.prevoir.org](http://www.prevoir.org); GMES-MACC program).

24 The CHIMERE model includes the MELCHIOR2 (*ModEle CHImique de l'Ozone à l'échelle*  
25 *Régionale*) chemical mechanism (around 40 species and 120 reactions) for the gas-phase chemistry,  
26 some aqueous-phase (e.g. aqueous pathways for sulfate production) and heterogeneous (e.g.  $\text{HNO}_3$   
27 formation on existing particles and fog droplets, including the conversion of  $\text{N}_2\text{O}_5$ ) reactions, and  
28 size dependent aerosol compounds (9 bins ranging from 40 nm to 20  $\mu\text{m}$  diameters), including  
29 secondary organic and inorganic aerosols. Dry and wet deposition of gaseous and aerosol species is  
30 parameterized from three types of sequential resistances following the resistance analogy (Wesely,  
31 1989). An aerodynamical resistance is estimated based on turbulent parameters (e.g. Monin-  
32 Obukhov length, friction velocity, dynamical roughness length). A quasi-laminary boundary layer  
33 resistance is calculated based on the molecular diffusivity of water and gaseous species and Prandtl  
34 number. The surface resistance of vegetation and soils is estimated from several parallel resistances  
35 related to plant surfaces via opening of stomata, and related to non-stomatal deposition at plant and



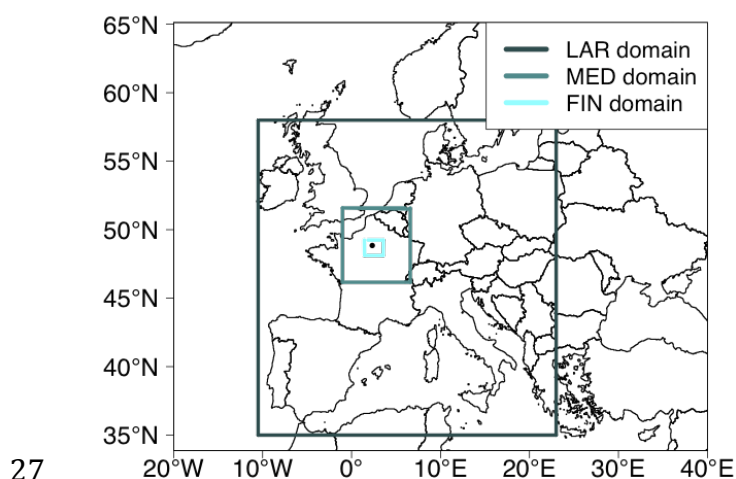
1 soil surfaces (Erisman et al., 1994). The scavenging of gases and particles, both in clouds and rain  
2 droplets, is included in CHIMERE. The scavenging of HNO<sub>3</sub> and NH<sub>3</sub> by cloud droplets (in rain  
3 droplets) is assumed reversible (irreversible). In clouds, particles can be scavenged by coagulation  
4 with cloud droplets or by precipitation, or can act as cloud condensation nuclei to form new  
5 droplets. Particles can also be scavenged by raining drops below the clouds. More details can be  
6 found in Menut et al. (2013). The model also includes a parameterization for the coagulation,  
7 absorption and nucleation aerosol processes.

8 Inorganic species are treated using the ISORROPIA thermodynamic equilibrium model (Nenes et  
9 al., 1998), considering only the NH<sub>3</sub>-HNO<sub>3</sub>-H<sub>2</sub>SO<sub>4</sub>-H<sub>2</sub>O system. ISORROPIA follows a bulk  
10 aerosol approach (without any consideration of the aerosol size distribution) and assumes an  
11 instantaneous equilibrium in the gas-aerosol system, as well as no influence of other compounds (in  
12 particular, the soluble organic matter). Given the temperature, RH, TNO<sub>3</sub>, TNH<sub>3</sub> and TS (assuming  
13 that TS=SO<sub>4</sub><sup>2-</sup> due to low concentrations of H<sub>2</sub>SO<sub>4</sub> and HSO<sub>3</sub> in the aerosol phase), the partitioning  
14 coefficient between both aerosol and gas phases at equilibrium is computed and used to drive the  
15 system toward the corresponding direction (thus countering the hypothesis of an instantaneous  
16 equilibrium assumed in ISORROPIA). For calculation efficiency, the model is not used on-line but  
17 through a tabulated version designed to cover a large range of meteorological conditions with  
18 temperature ranging from 260 to 312 K (increment +2.5 K), RH from 0.3 to 0.99 (increment +0.05)  
19 and TS, TNO<sub>3</sub> and TNH<sub>3</sub> concentrations from 10<sup>-2</sup> to 65 μg m<sup>-3</sup> (increment x1.5) (Menut et al.,  
20 2013).

21

## 22 **3.2 Model configuration**

23 As shown in Fig. 1, three nested domains are used for all simulations — a large (LAR), a medium  
24 (MED) and a fine (FIN) domain —, with horizontal resolutions increasing from 0.5 x 0.5° (roughly  
25 50 x 50 km), 9 x 9 km and 3 x 3 km, respectively. A discretization of 8 levels, from 40 m to 5 km  
26 a.g.l., is applied on the vertical dimension.



1 Figure 1: Nested domains (the black points in the finest domain indicates Paris). Resolutions are  
2  $0.5 \times 0.5^\circ$  (LAR domain),  $9 \times 9$  km (MED) and  $3 \times 3$  (FIN).  
3 Meteorological inputs are provided by PSU/NCAR MM5 simulations (Dudhia, 1993) using  
4 boundary conditions and large scale data coming from the Final Analyses (FNL) data from the  
5 National Centers for Environmental Prediction (NCEP) (<http://rda.ucar.edu/datasets/ds083.2>).  
6 Gaseous and aerosol emissions in all domains come from the so-called TNO-MP (MP for  
7 MegaPoli) inventory. Developed in the framework of the European MEGAPOLI (Megacity:  
8 emission, urban, regional and global atmospheric pollution and climate effect, and integrated tools  
9 for assessment and mitigation ; [www.megapoli.info](http://www.megapoli.info)) project (Baklanov et al., 2010), this highly-  
10 resolved ( $0.125 \times 0.0625^\circ$ , i.e. roughly  $7 \times 7$  km) European inventory is based on the TNO  
11 inventory (Gon et al., 2010; Pouliot et al., 2012; Kuenen et al., 2014), but incorporates bottom-up  
12 emission data (compiled by local authorities such as Airparif for Paris (Airparif, 2010)) over the  
13 four European megacities (Paris, London, Rhine-Ruhr and Po valley) (see Denier van der Gon et  
14 al., 2011 for more details). The region of Paris roughly corresponds to the FIN domain. In order to  
15 reach the CHIMERE resolution, emissions are downscaled based on the  $1 \times 1$  km-resolved GLCF  
16 (Global Land Cover Facility) land use database (Hansen et al., 2000), and apportioned according to  
17 the type of land use (Menut et al., 2013).  
18 Boundary and initial conditions come from the LMDz-INCA2 (Folberth et al., 2006) global model  
19 for gaseous species and the LMDZ-AERO (Folberth et al., 2006; Hauglustaine, 2004) for  
20 particulate species. Biogenic emissions are computed from the MEGAN model using  
21 parameterizations from Guenther et al. (2006).  
22 This reference simulation will be referred to as the MOD case. A second simulation is performed  
23 without any local anthropogenic emissions from the region of Paris (in the three nested domains), in  
24 order to assess the influence of imported pollution over the city of Paris. It will be referred to as the  
25 MOD-noIDF case (IDF for Ile-de-France, the name of the region of Paris). In addition, as  $\text{NH}_3$  is  
26 strongly impacted by dry deposition in which high uncertainties persist (e.g. Flechard et al., 2011), a  
27 third simulation (so-called MOD-noddep) is performed without any  $\text{NH}_3$  dry deposition over the  
28 entire domain in order to investigate its influence on concentrations within Paris.

29 **4 Results**

30 The following subsections present results on sulfate and  $\text{SO}_2$  (Sect. 4.1),  $\text{NH}_3$  (Sect. 4.2) and  $\text{HNO}_3$   
31 (Sect. 4.3). For all compounds, the temporal variability given by measurements is assessed at  
32 different scales (monthly, daily and diurnal), as well as the model's ability to reproduce the  
33 observed concentrations. For the analysis of air mass origins, back-trajectories have been calculated  
34 during the whole period with the FLEXTRA model (Stohl et al., 2001) using the same MM5  
35 meteorology as in the CHIMERE simulations. The FLEXTRA simulations are performed by

1 releasing, every 6 hours, 10 particles around the center of Paris, starting at 500 m altitude, which  
 2 leads to a daily set of 40 back-trajectories. Several uncertainty sources in the model (or input data)  
 3 are also discussed. The nitrate formation regime in terms of limiting species among  $\text{NH}_3$  and  $\text{HNO}_3$ ,  
 4 the nitrate simulation in CHIMERE as well as the nitrate response to changes in precursors  
 5 concentrations are then characterized in Sect. 4.4.

6 Statistical metrics used in the evaluation of the CHIMERE results compared to observations are  
 7 defined as follows:

8 • Mean bias:  $MB = \frac{1}{n} \sum_{i=1}^n (m_i - o_i)$  (1)

9 • Normalized mean bias:  $NMB = \frac{\frac{1}{n} \sum_{i=1}^n (m_i - o_i)}{\bar{o}}$  (2)

10 • Root mean square error:  $RMSE = \sqrt{\frac{1}{n} \sum_{i=1}^n (m_i - o_i)^2}$  (3)

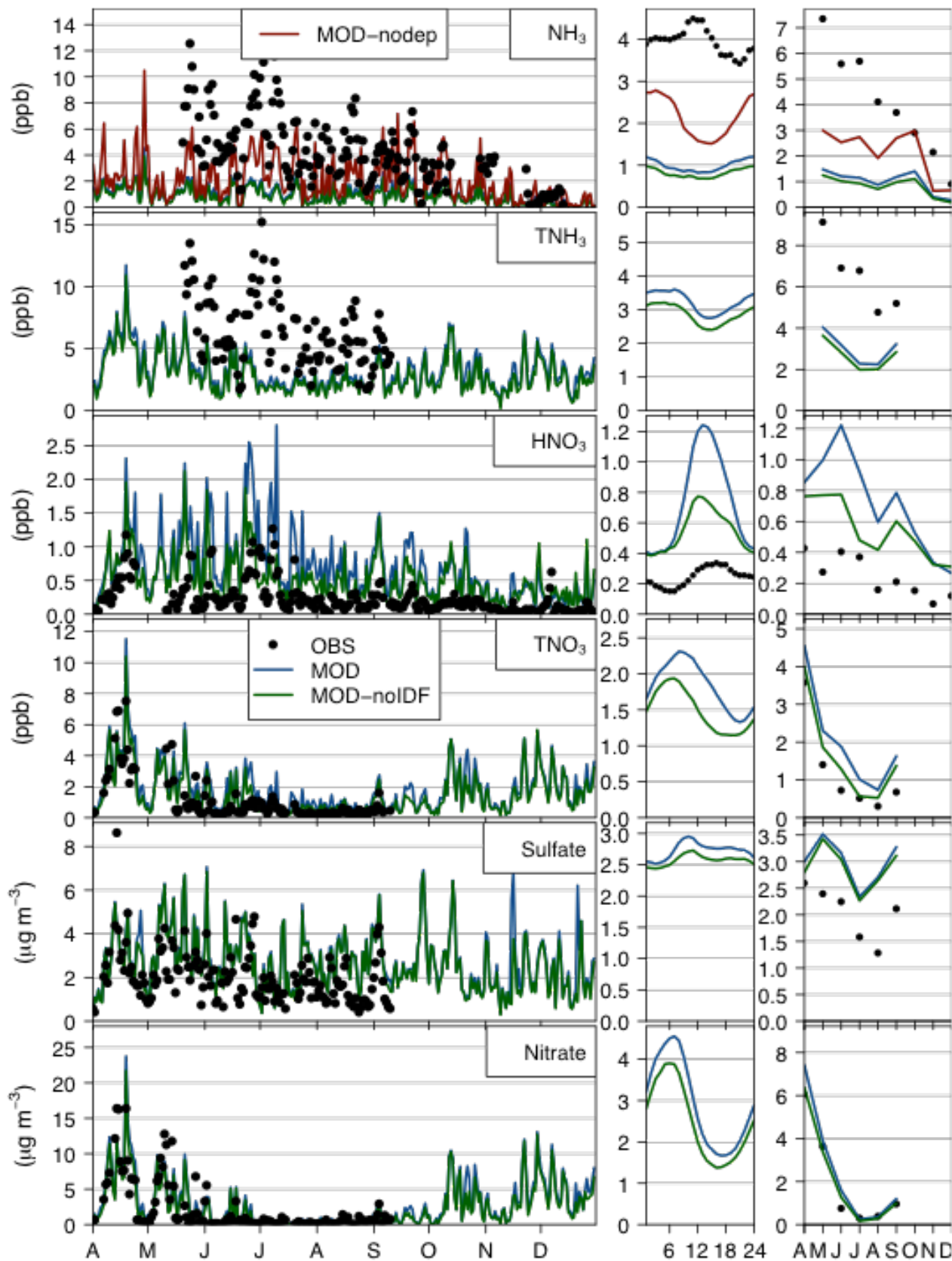
11 • Normalized root mean square error:  $RMSE = \frac{\sqrt{\frac{1}{n} \sum_{i=1}^n (m_i - o_i)^2}}{\bar{o}}$  (4)

12 • Correlation coefficient:  $R = \frac{\sum_{i=1}^n (m_i - \bar{m})(o_i - \bar{o})}{\sqrt{\sum_{i=1}^n (m_i - \bar{m})^2 \sum_{i=1}^n (o_i - \bar{o})^2}}$  (5)

13 With  $m_i$  and  $o_i$  being the modelled and observed concentrations at time  $i$ , respectively, and  $\bar{m}$   
 14 and  $\bar{o}$  their average over a given period.

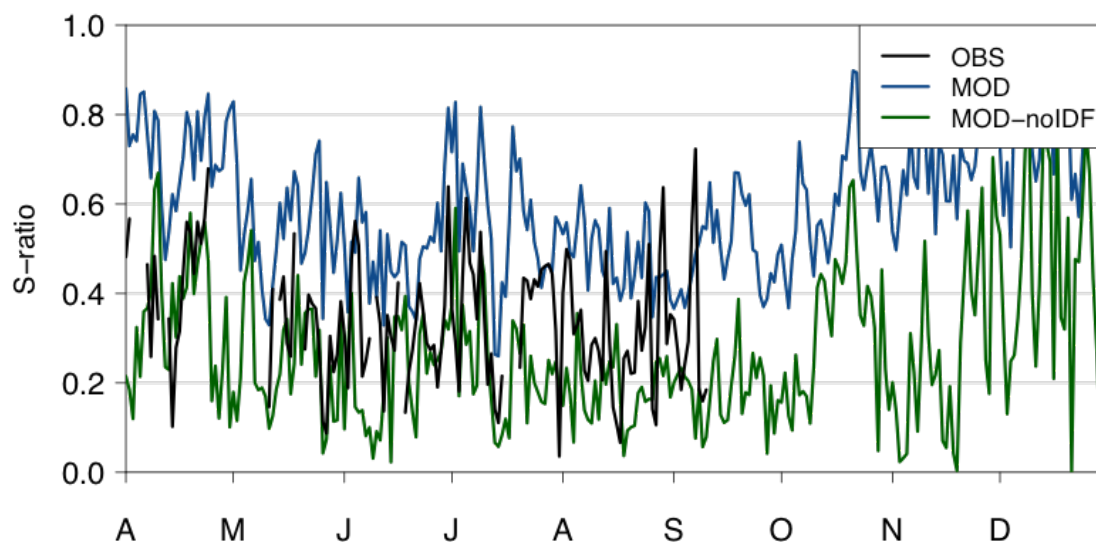
#### 15 **4.1 Sulfate and $\text{SO}_2$**

16 Sulfate daily concentrations in Paris are given in Fig. 2. The variability of sulfate (as of nitrate)  
 17 during the PARTICULES campaign has been discussed in details in Bressi et al. (2013). Fine  
 18 ( $\text{PM}_{2.5}$ ) sulfate concentrations range between 0.4 and 5.0  $\mu\text{g m}^{-3}$  (one high value at 8.7  $\mu\text{g m}^{-3}$ ), with  
 19 an average of 2.0  $\mu\text{g m}^{-3}$  over the studied period (1 April – 10 September). The episodes with  
 20 highest concentrations are associated with air masses originating from the North/North-East, also  
 21 noted by Bressi et al. (2013), Petetin et al. (2014) and Petit et al. (2015). Despite a faster  $\text{SO}_2$ -to-  
 22 sulfate conversion due to higher OH levels in summer, lower concentrations are measured during  
 23 that season due to a combination of lower  $\text{SO}_2$  emissions and a dominant marine regime, with  
 24 relatively clean air masses originating from west and southwest and slightly more polluted ones  
 25 from northwest.



1  
 2 Figure 2: Observed and modelled daily averaged concentrations (left panel), diurnal profiles  
 3 (middle panel), and monthly concentrations (right panel). MOD-nodep results are only shown for  
 4  $\text{NH}_3$ . Note: CHIMERE monthly concentrations are computed including only days with available  
 5 observational data. For particulate matter observations, only daily values are available.

1 During the period of available data (152 days in spring and summer),  $\text{NH}_3$  levels are high enough to  
 2 fully neutralize both sulfate and nitrate, as indicated by the linear regression of  $\text{NH}_4^+$  versus  $\text{NO}_3^-$   
 3  $+2\text{SO}_4^{2-}$  daily concentrations in the fine mode that gives a slope of 1.01, a y-intercept of -0.20 ppb  
 4 and a correlation coefficient ( $r^2$ ) of 0.97 ( $n=150$ ; see Fig. S1 in the Supplement). Note that plotting  
 5 all major cations ( $\text{Na}^+ + \text{NH}_4^+ + \text{K}^+ + 2\text{Ca}^{2+} + 2\text{Mg}^{2+}$ ) against all major anions ( $\text{NO}_3^- + 2\text{SO}_4^{2-} + \text{Cl}^-$ ) leads  
 6 to a slope of 1.03, a y-intercept of +0.13 ppb and a correlation of 0.97, demonstrating the neutrality  
 7 of our fine aerosol.



8  
 9 Figure 3: Observed and modelled (with – MOD case – and without – MOD-noIDF case – emissions  
 10 over the Paris region) daily S-ratio in Paris.

11 Statistical results of modelled versus measured concentrations are reported in Table 1. The model  
 12 partially reproduces the day-to-day variability of sulfate concentrations ( $r=0.59$ ), but overestimates  
 13 concentrations, with a NMB of +48% and a NRMSE of 74%. This does not appear to be related to a  
 14 too high  $\text{SO}_2$ -to-sulfate conversion since  $\text{SO}_2$  concentrations are significantly overestimated in  
 15 Paris, by about a factor of 3 (Table 1). This is also suggested by the simulated S-ratio. This  
 16 indicator – defined as the ratio of  $\text{SO}_2$  over  $\text{SO}_2 + \text{SO}_4^{2-}$ , all concentrations being expressed in  $\mu\text{g m}^{-3}$   
 17 (Hass et al., 2003; Pay et al., 2012) – allows to assess how strongly oxidized is a plume containing  
 18 sulfur. High S-ratios are found in air masses containing freshly emitted  $\text{SO}_2$ , while low S-ratios are  
 19 associated with older air masses in which more  $\text{SO}_2$  has already been converted into sulfate. The  
 20 observed and simulated S-ratios are shown in Fig. 3 (the  $\text{SO}_2 + \text{SO}_4^{2-}$  time series is shown in Fig. S4  
 21 in the Supplement). In the MOD simulation, CHIMERE clearly overestimates the S-ratio (average  
 22 value of 0.54 versus 0.34 for the observations), i.e. the simulated air masses contain too much  
 23 freshly emitted  $\text{SO}_2$  compared to reality. Such a high bias on  $\text{SO}_2$  concentrations is not expected,  
 24 but does not appear representative of the CHIMERE performance at a larger scale. Considering the  
 25  $\text{SO}_2$  observations available at 9 urban background sites (AIRPARIF operational network) in the  
 26 region of Paris, NMB are lower, ranging from +24 to +160%. As a large part of  $\text{SO}_2$  is emitted by  
 27 point sources, the dilution effect in a 3 x 3 km cell remains a well-known uncertainty source at

1 stations potentially impacted by plumes coming from nearby industrial facilities. However, in our  
2 case, large SO<sub>2</sub> industrial point sources are relatively far from our background urban station, and  
3 emissions from non-point sources (i.e. on-road transport and residential sectors) remain important in  
4 the center of Paris, which suggests potential errors on the Paris agglomeration emissions  
5 (overestimation of total emissions, wrong vertical allocation) and/or the BLH. Indeed, the average  
6 SO<sub>2</sub> diurnal profile shows maximum discrepancies (up to a factor of 4.8) during the transition from  
7 a convective to a nocturnal boundary layer. This transition occurs too early in the model (see Fig.  
8 S3 in the Supplement), which likely explains a noticeable part of the bias for SO<sub>2</sub>. Conversely, the  
9 sulfate overestimation may be due to errors during the transport of air masses from North-Eastern  
10 Europe.

11 Table 1: Statistical results at our urban background sites over the whole period (all statistical  
12 metrics are defined at the beginning of Sect. 4; MO is the observed concentration mean, N the data  
13 coverage).

Species	Case	MO	NMB		NRMSE			
			MB	(%)	RMSE	(%)	R	N (%)
NH <sub>3</sub> * (ppb)	MOD	4.0	-3.0	-75	3.9	99	0.42	64
	MOD-noIDF		-3.1	-79	4.1	103	0.39	64
	MOD-noddep		-1.8	-46	3.2	82	0.45	64
HNO <sub>3</sub> * (ppb)	MOD	0.3	+0.5	+195	0.8	320	0.56	81
	MOD-noIDF		+0.3	+120	0.6	219	0.36	81
SO <sub>2</sub> * (ppb)	MOD	0.5	+1.0	+194	1.6	303	0.38	83
	MOD-noIDF		-0.1	-20	0.9	170	0.25	83
Ammonium (μg m <sup>-3</sup> )	MOD	1.2	+0.4	+35	0.9	70	0.84	54
	MOD-noIDF		+0.3	+23	0.8	64	0.84	54
Nitrate (μg m <sup>-3</sup> )	MOD	2.1	+0.4	+19	2.2	109	0.81	54
	MOD-noIDF		+0.0	+1	2.1	101	0.81	54
Sulfate (μg m <sup>-3</sup> )	MOD	2.0	+1.0	+48	1.5	74	0.59	54
	MOD-noIDF		+0.9	+42	1.4	69	0.61	54
F-NH <sub>x</sub> (ppb)	MOD	5.5	-4.1	-75	4.7	87	0.51	37
	MOD-noIDF		-4.4	-80	5.0	92	0.48	37
S-ratio	MOD	0.3	+0.2	+60	0.3	73	0.46	48
	MOD-noIDF		-0.1	-29	0.2	55	0.33	48
GR (ppb ppb <sup>-1</sup> )	MOD	12.6	-11.4	-90	14.2	112	0.37	36
	MOD-noIDF		-11.2	-88	14.0	111	0.33	36

TNH <sub>3</sub> (ppb)	MOD	6.4	-3.6	-56	4.4	70	0.43	37
	MOD-noIDF		-3.9	-61	4.7	74	0.40	37
TNO <sub>3</sub> (ppb)	MOD	1.1	+0.8	+71	1.3	123	0.78	47
	MOD-noIDF		+0.3	+31	1.1	97	0.79	47

1 \* Statistics based on hourly data (otherwise, daily data are used).

## 2 **4.2 Ammonia**

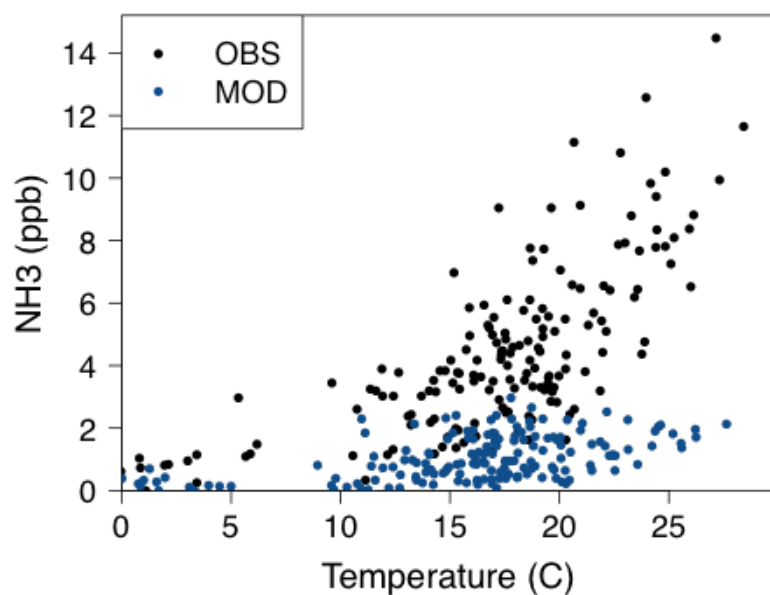
### 3 **4.2.1 Temporal variability**

4 Daily averaged concentrations and diurnal profiles of NH<sub>3</sub> are given in Fig. 2. The model results  
5 will be discussed in the next section. According to the review of Reche et al. (2012), NH<sub>3</sub>  
6 concentrations in worldwide urban environments range between 0.4 and 63.6 ppb, thus spanning  
7 over two orders of magnitude. On a logarithmic scale, the average concentration of 4.0 ppb  
8 measured in Paris over the whole period is roughly in the middle range of this range. It is also  
9 consistent with the values obtained in other European cities: 4.4 ppb in Aveiro (Portugal, August-  
10 May), 5.2 ppb in Roma (Italy, May-March), 5.5 ppb in Münster (Germany, May-June), 3.2 in  
11 Thessaloniki (Greece, year), 3.9-10.6 in Barcelona (Spain, July and January), 3.1 ppb in Schiedam  
12 (The Netherlands, winter) (Reche et al., 2012 and references therein). NH<sub>3</sub> concentrations in Paris  
13 show a large variability (illustrated by a standard deviation of 2.8 ppb) with several elevated NH<sub>3</sub>  
14 episodes in late spring and early summer (hourly concentrations reaching up to 18.5 ppb in June),  
15 moderate concentrations in late summer and lower ones in autumn and winter. On average, the  
16 observed NH<sub>3</sub> diurnal profile (Fig. 2) is rather flat, with slightly increasing concentrations in the  
17 morning leading to a maximum at 10:00-13:00 UTC. Concentrations decrease in the afternoon up to  
18 a minimum at 20:00 UTC. The diurnal variability of NH<sub>3</sub> depends on many factors, including the  
19 strength of local emission sources, the dry deposition, the evolution of the BLH, the formation of  
20 NH<sub>4</sub>NO<sub>3</sub> during the night promoted by larger RH and its thermodynamically driven evaporation  
21 during the daytime (Wichink Kruit et al., 2007). The daytime increase may be partly due to this  
22 volatilization of NH<sub>4</sub>NO<sub>3</sub>.

#### 23 **4.2.1.1 Influence of temperature**

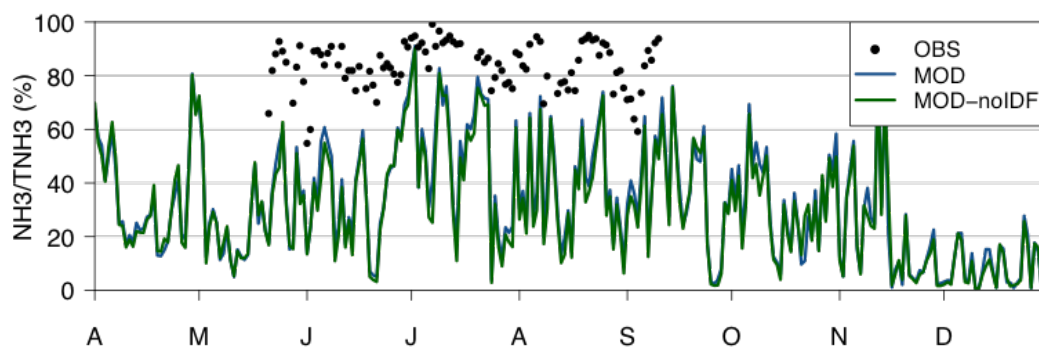
24 Figure 4 shows the NH<sub>3</sub> concentrations in function of the temperature. Both appear clearly linked in  
25 Paris, the highest episodes occurring concomitantly with the warmest conditions (see the  
26 meteorology evaluation in the Supplement, Sect. S.2). The lower sensitivity to temperature in the  
27 model will be discussed later. Such a relation between NH<sub>3</sub> and the temperature has already been  
28 observed in other cities (e.g. Perrino et al., 2002; Gong et al., 2011; Reche et al., 2012).  
29 Temperature and RH strongly influence the equilibrium constant governing the partitioning of  
30 inorganic compounds between the gas and aerosol phases, with higher NH<sub>3</sub> concentrations expected

1 when the temperature is high and the RH is low, due to the volatilization of  $\text{NH}_4\text{NO}_3$ . In addition,  
 2 several  $\text{NH}_3$  emission sources may be enhanced by high temperature, including the agricultural (e.g.  
 3 volatilization of fertilizer) or biological sources.



4  
 5 Figure 4: Daily observed (in black) and modelled (in blue)  $\text{NH}_3$  concentrations versus temperature  
 6 in Paris (for the model, only days with available observations are plotted).

7 The link between  $\text{NH}_3$  and temperature can be illustrated by the early July episode when, in parallel  
 8 with the temperature increase between 30 June and 2 July, the  $\text{NH}_3$  baseline progressively increases  
 9 in Paris, up to 18.5 ppb at the hourly scale (the maximum over the whole FRANCIPOL period). A  
 10 part of the  $\text{NH}_3$  increase is likely due to evaporation of  $\text{NH}_4\text{NO}_3$  but in early July, a similar episode  
 11 is observed for  $\text{TNH}_3$ , which means that an additional  $\text{NH}_3$  source is present. The  $\text{NH}_3/\text{TNH}_3$  ratios  
 12 are shown in Fig. 5. The experimentally determined  $\text{TNH}_3$  is clearly dominated by  $\text{NH}_3$  that has a  
 13 contribution around 55-99% (83% on average). Negative artefacts on the  $\text{NH}_4^+$  filter measurements  
 14 cannot be excluded (in particular during summertime), but increasing  $\text{NH}_4^+$  concentrations by 50%  
 15 has a very limited impact ( $\text{NH}_3$  contributions ranging in that case around 45-99%, and 78% on  
 16 average).

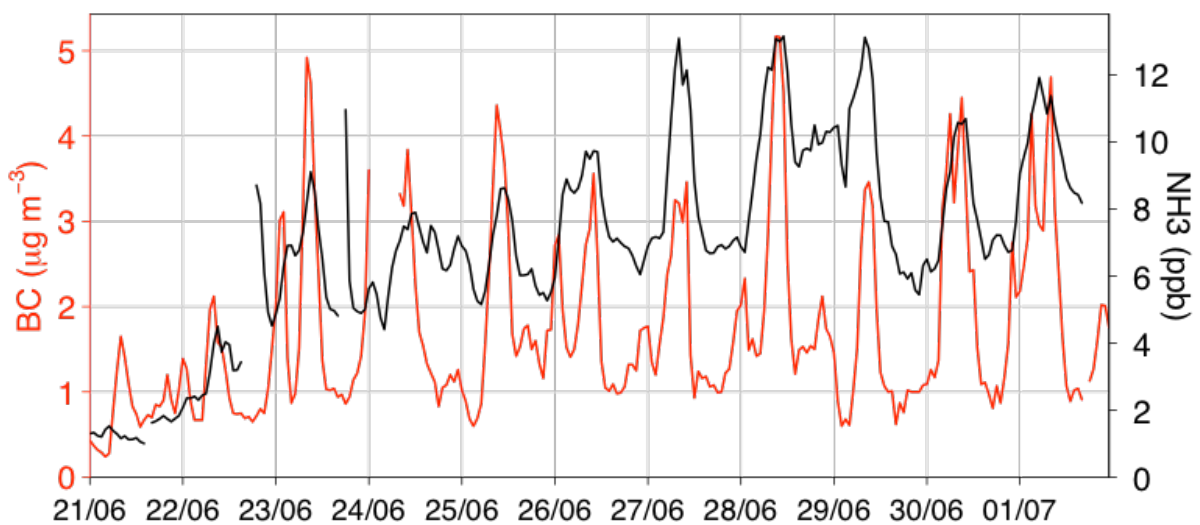


17  
 18 Figure 5: Daily  $\text{NH}_3/\text{TNH}_3$  ratios in observations (points) and simulations (solid lines).



#### 1 4.2.1.2 Influence of traffic NH<sub>3</sub>

2 Several studies have previously addressed the question of the NH<sub>3</sub> emitted by the traffic in urban  
3 areas, although with more or less contrasted and definitive conclusions depending on the city (e.g.  
4 Perrino et al., 2002; Gong et al., 2011). The difficulty notably arises from the short lifetime of NH<sub>3</sub>  
5 that can quickly deposit on the ground, be diluted or converted into NH<sub>4</sub><sup>+</sup>. In Paris, the diurnal  
6 profile does not show any peak at morning and evening rush hours, even during periods of lower  
7 agricultural emissions (e.g. August and September; too few data in winter). This suggests that  
8 traffic emissions are probably a relatively minor source during our study. This is supported by the  
9 low correlation of black carbon (BC) (mainly emitted by the traffic) and NH<sub>3</sub> concentrations  
10 measured at the LHVP site (r=0.20 over the whole period). However, it is worth noting that during  
11 the end of June episode, the hourly time series shows some morning peaks (above an increasing  
12 background line likely due to the advection of agricultural NH<sub>3</sub>) that may be associated to traffic  
13 NH<sub>3</sub> emissions, as illustrated by the increased correlation with BC (r=0.60 between the 21 June and  
14 3 July) (Fig. 6). No similar situation is observed during the rest of the campaign. In Roma, Perrino  
15 et al. (2002) observed high levels of NH<sub>3</sub> at curbside sites with a diurnal profile clearly influenced  
16 by traffic emissions. But due to the combined action of dry deposition, dilution after emissions as  
17 well as the conversion into particulate NH<sub>4</sub><sup>+</sup> (with sulfates and/or nitrates), these concentrations  
18 were severely reduced at the urban background scale (about a factor of 5) and the traffic profile type  
19 had disappeared. As a result, our urban background conditions may have prevented us from  
20 accurately assessing the potential impact of traffic emissions on ambient NH<sub>3</sub> concentrations.  
21 Investigating the NH<sub>3</sub> diurnal variability at the SIRTAs site, Petit et al. (2015) noticed a bimodal  
22 traffic-like variation but only during spring and not during summer and winter, suggesting that these  
23 variations may be related to processes other than traffic.



24  
25 Figure 6: Observed BC (in red) and NH<sub>3</sub> (in black) hourly concentrations at LHVP during the end  
26 of June.

27

### 1 **4.2.1.3 Influence of agricultural NH<sub>3</sub>**

2 As previously mentioned, NH<sub>3</sub> is emitted by both agricultural and non-agricultural sources. The  
3 former clearly dominates at the national scale, as well as at the scale of the Paris region (which  
4 includes the rural areas surrounding Paris), while the latter dominates at the scale of the city itself  
5 (which includes only urban areas). Considering the role of NH<sub>3</sub> in the formation of NH<sub>4</sub>NO<sub>3</sub> and the  
6 important contribution of this aerosol compound to the PM<sub>2.5</sub> pollution in Paris, it is of major  
7 importance to assess the relative contribution of both types of sources to the NH<sub>3</sub> urban background  
8 in the city. Answering that question would ideally require additional NH<sub>3</sub> observations in Paris and  
9 its surroundings in order to quantify the increment associated to local sources. Without such  
10 observations, it is not possible to quantitatively investigate the NH<sub>3</sub> budget in Paris.

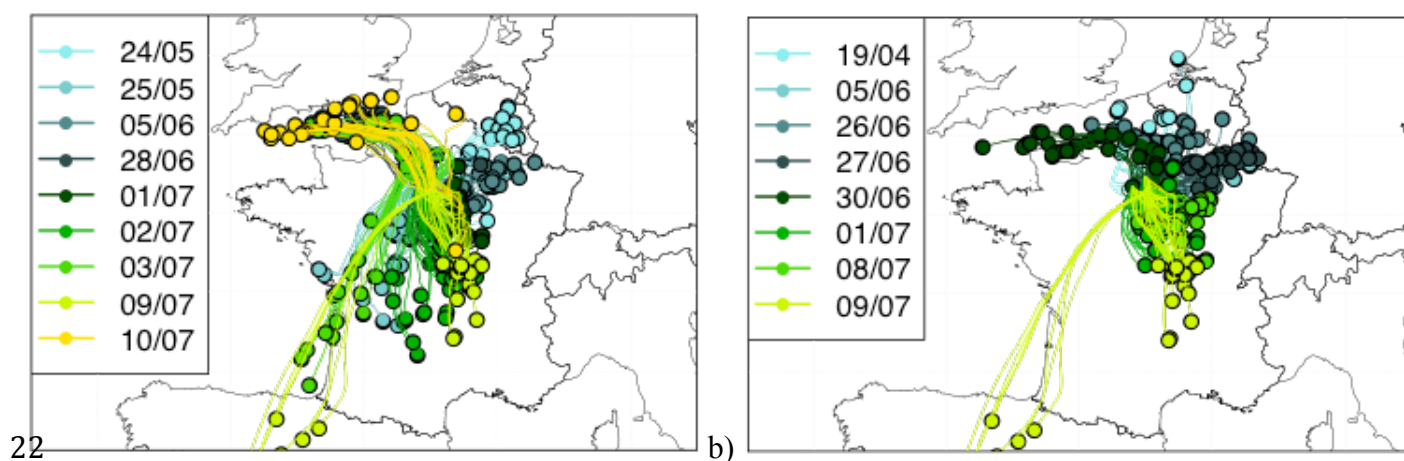
11 However, based on the available observations, we argue in this section that among all NH<sub>3</sub> emission  
12 sources, agriculture is probably the main driver of the day-to-day variability of NH<sub>3</sub> concentrations  
13 in Paris during the time of the campaign (from spring to autumn) (in conjunction with the  
14 thermodynamic equilibrium that drives the partitioning between the gas and aerosol phases).

15 This is mainly supported by the NH<sub>3</sub> (and TNH<sub>3</sub>) seasonal variations. Although incomplete (due to  
16 missing observations in winter and early spring), the NH<sub>3</sub> seasonal pattern shows a maximum in  
17 spring and early summer, moderate concentrations in late summer and a minimum in autumn. Such  
18 a seasonal pattern has been already reported in several studies (e.g. Reche et al., 2012; Skjøth et al.,  
19 2011). A roughly similar variability is expected for the fertilizer applications. Yet this emission  
20 source represents around 40% of the total agricultural source at the national scale, and this  
21 contribution appears even higher around the Paris region (Hamaoui-Laguel et al., 2014; see in  
22 particular their Fig. 2a and 2b). The observed increase of NH<sub>3</sub> with temperature is also compatible  
23 with this source, as increased temperature favors fertilizer evaporation (e.g. Hamaoui-Laguel et al.,  
24 2014). Conversely, none of the non-agricultural emission sources is expected to be particularly  
25 intense during this time of the year. This was discussed for traffic related emissions in the last  
26 section. Some NH<sub>3</sub> may also be emitted by biomass burning (for residential heating) but these  
27 emissions are, in any case, low in spring and summer. Emissions from sewage and waste disposal as  
28 well as emissions from other biological sources may also contribute to NH<sub>3</sub> levels. Interestingly,  
29 these latter sources may be influenced by temperature, as are the NH<sub>3</sub> concentrations measured in  
30 Paris (see Fig. 4). But if they dominate, one would not expect such a large difference in  
31 concentrations between late May, early June and August (when temperatures were comparable).  
32 Additionally, in this case, one would also expect higher NH<sub>3</sub> concentrations during stagnant  
33 conditions, which is in contradiction with the low correlation between BC and NH<sub>3</sub> (given that such  
34 stagnant conditions lead to an accumulation of BC). The NH<sub>3</sub> diurnal profile shows very limited  
35 variations along the day, which is consistent with the idea of a strong NH<sub>3</sub> background originating  
36 from agricultural sources around the Paris region. All these elements thus suggest that the

1 agricultural source (and more precisely the fertilizer application) drives a larger part of the  $\text{NH}_3$   
2 day-to-day variability in Paris than the other emission sources.

### 3 4.2.1.4 Geographical origin of the highest $\text{NH}_3$ episodes

4 In this section, we investigate the geographical origin of the air masses associated with elevated  
5  $\text{NH}_3$  episodes. Back-trajectories during the 10 days of highest  $\text{NH}_3$  concentrations (daily averages  
6 above 9.2 ppb, the 95<sup>th</sup> percentile of all daily values) are presented in Fig. 6a. Most  $\text{NH}_3$  episodes  
7 are associated with moderate winds at altitude (particles being released at 500 m a.g.l. in FLEXTRA  
8 simulations), air masses at D-1 (one day before reaching Paris) being located in a radius of 50-400  
9 km from Paris. A noticeable exception is found on 9 July in the morning (around 6 UTC) when the  
10 wind suddenly changes direction (from Southeast to Southwest) and speed (getting much stronger,  
11 with air masses originating from Spain at D-1) while  $\text{NH}_3$  concentrations increase. Interestingly,  
12 some of the highest  $\text{NH}_3$  episodes (e.g. 10 July) are associated with oceanic air masses (excepted to  
13 be relatively clean) that have spent only a limited time over land, which suggests the presence of  
14 intense  $\text{NH}_3$  emissions in the corresponding regions (Normandy). The trajectory analysis suggests  
15 that air masses with high  $\text{NH}_3$  concentrations do not appear to originate from a particular  
16 geographical region. Instead, the highest episodes appear linked to more diffuse  $\text{NH}_3$  emissions in  
17 the northern part of France, associated with anticyclonic conditions with high temperature and  
18 moderate winds. This is in accordance with Petit et al. (2015) that suggest, based on  $\text{NH}_3$   
19 measurements at the SIRTA suburban site (southwest of Paris), a diffuse regional  $\text{NH}_3$  source, in  
20 particular during summer (in spring, some high  $\text{NH}_3$  episodes associated to E/NE/SE winds are also  
21 noticed, but without any clear pattern).



23 Figure 6: Back-trajectories at D-1 (one day before reaching Paris) associated with highest (a)  $\text{NH}_3$   
24 (left panel) and (b)  $\text{HNO}_3$  (right panel) episodes (highest episodes being selected according to daily  
25 concentrations above the 97<sup>th</sup> percentile of all daily measurements, i.e. 9.2 and 0.9 ppb for  $\text{NH}_3$  and  
26  $\text{HNO}_3$ , respectively). For clarity, only back-trajectories of 7 particles around the center of Paris are  
27 plotted, each 6 h (i.e. 28 back-trajectories per day).

## 1 4.2.2 Model results

2 As shown in Fig. 2, NH<sub>3</sub> concentrations are significantly underestimated by the CHIMERE model  
3 with a NMB of -75% (see statistical results in Table 2). This negative bias not only affects the  
4 intense peaks but also the baseline concentrations. In their evaluation of the CALIOPE-EU  
5 modelling system, Pay et al. (2012) reviewed the statistical results of various regional models over  
6 Europe (during a whole year for most models). As our study does not cover a whole year, statistical  
7 results are not directly comparable, but figures still shed light on the relative performance of our  
8 CHIMERE simulation. The negative bias in our study is in the range of those reported by Pay et al.  
9 (2012) where NMB varied from -82 to -15 %. Our RMSE (3.9 ppb) is among the best values  
10 reported by Pay et al. (2012) (1.6 ppb for the CALIOPE-EU model and 7.6-10.6 ppb for the six  
11 other models), as well as the correlation (0.42 versus 0.05-0.56). Nevertheless, the CHIMERE  
12 model dramatically fails to reproduce the strong spring and summer episodes (and consequently the  
13 seasonal variation) during which negative biases on daily concentrations can exceed a factor of 10,  
14 despite a monthly distribution of emissions peaking between March and May (spring fertilizer  
15 application).

16 The similar results obtained in the MOD and MOD-noIDF cases indicate that most of the simulated  
17 NH<sub>3</sub> originates from outside the region of Paris. Concentration maps show that simulated NH<sub>3</sub>  
18 concentrations closely follow the spatial distribution of emissions, with maximum levels over  
19 Brittany, North of France and Benelux. Due to both dilution and deposition, NH<sub>3</sub> concentrations  
20 quickly decrease with distance from these source regions. However, the simulated NH<sub>3</sub> lifetime  
21 appears high enough to allow imports over the region of Paris. As an illustration, highest simulated  
22 concentrations in the city (4.5 ppb, the 29<sup>th</sup> April) result from the advection of air masses from  
23 Eastern Brittany and South-West during the month of maximum emissions (according to monthly  
24 factors applied to emissions).

25 Comparing observations and model results at the MONTSOURIS meteorological station, a negative  
26 bias for temperature (-1.6°C) and a positive bias for RH (+5.9% in absolute) (see Sect. S.2 in the  
27 Supplement) is noted. This favors the formation of NH<sub>4</sub><sup>+</sup> and thus decreases gaseous NH<sub>3</sub> in TNH<sub>3</sub>.  
28 However, correcting these errors in the ISORROPIA model (i.e. replacing the simulated  
29 temperature and RH values with measured values, without modifying TNH<sub>3</sub>, TNO<sub>3</sub> and TS  
30 concentrations) does not fill the gap with observations (the average NH<sub>3</sub> concentrations increasing  
31 by only 7% on average). Errors may be larger close to the deliquescence point where the influence  
32 of RH is stronger. The deliquescent RH (DRH) of NH<sub>4</sub>NO<sub>3</sub> and (NH<sub>4</sub>)<sub>2</sub>SO<sub>4</sub> at 298K are 61.8 and  
33 79.9%, respectively (Seinfeld and Pandis, 2006). A mixture of both salts will have a DRH between  
34 these two extreme values. Focusing on days where RH ranges between 60 and 80% (i.e. close to the  
35 deliquescent point of the mixture), the average NH<sub>3</sub> increase is even lower (6%). It reaches 14%

1 when considering RH between 60 and 65%. In any case, the impact remains limited. As shown in  
2 Fig. 5, the fraction of  $\text{NH}_3$  in  $\text{TNH}_3$  simulated by CHIMERE is highly variable, ranging from less  
3 than 5% to about 90%, in contradiction with observations which show a clear gas phase reservoir  
4 during spring and summer (at around 60-100%). The already mentioned overestimation of  $\text{SO}_4^{2-}$  in  
5 CHIMERE (see Sect. 4.1) may directly reduce the amount of  $\text{NH}_3$  available in the gas phase.  
6 However, the bias on  $\text{TNH}_3$  is only reduced to -56% (against -76% for  $\text{NH}_3$  alone), which indicates  
7 that only a minor part of the negative bias on  $\text{NH}_3$  can be explained by an erroneous partitioning  
8 between both gas and aerosol phases (including errors related to  $\text{SO}_4^{2-}$ ).

9 Although not likely the main  $\text{NH}_3$  source (see Sect. 4.2.1.3), the traffic can also contribute to the  
10  $\text{NH}_3$  urban background levels in Paris. Yet in the TNO-MP inventory, these traffic emissions are  
11 missing in the Paris region (but not outside this region) (see Table S3 in the Supplement), which  
12 may induce an underestimation of modelled  $\text{NH}_3$  concentrations. The contribution of traffic to  
13 ambient  $\text{NH}_3$  levels in urban environments is highly variable from one city to another, as illustrated  
14 by the  $\text{NH}_3/(\text{NH}_3+\text{NO}_x)$  emission molar ratios that range from a few percent (Yao et al., 2013) to a  
15 few tens of percent (Bishop et al., 2010) which are due to differences in the vehicle fleet (Carslaw  
16 and Rhys-Tyler, 2013). Several sensitivity tests were performed with added  $\text{NH}_3$  traffic emissions,  
17 derived from the  $\text{NO}_x$  traffic emissions with  $\text{NH}_3/(\text{NH}_3+\text{NO}_x)$  conversion factors in the range of the  
18 values given in the literature : 1, 6, 12 and 18% (not shown). Such additional emissions reduce the  
19 bias, but do not improve the correlation between model and measurements. In particular, they  
20 induce a clear increase of  $\text{NH}_3$  concentrations during the morning and evening rush hours, which is  
21 not in agreement with the observed diurnal profile. These results thus prevent us from concluding  
22 on the importance of these traffic emissions on  $\text{NH}_3$  urban background levels.

23 A large part of the model errors probably arises from the representation of  $\text{NH}_3$  air-surface  
24 exchanges (agricultural emissions and deposition) in the CHIMERE model. This representation is  
25 by far too simplistic in several respects: (i) the parameterization of  $\text{NH}_3$  dry deposition is uni-  
26 directional and does not take into account the compensation with emissions; (ii) the agricultural  
27 emissions are temporally disaggregated based on monthly, day-of-the-week and diurnal factors  
28 without taking into account any environmental factor (e.g. air temperature, soil moisture,  
29 agricultural practices) known to influence some  $\text{NH}_3$  emissions (e.g. the volatilization of fertilizers).  
30 This likely explains the much lower  $\text{NH}_3$ -temperature correlation obtained in the model in  
31 comparison with observations ( $r=0.52$  against 0.72 in observations), as illustrated in Fig. 4. In light  
32 of our comparison, the parameterization of the  $\text{NH}_3$  emissions in CHIMERE cannot represent the  
33 high spatio-temporal variability of  $\text{NH}_3$  concentrations, and in particular fails in reproducing the  
34 large  $\text{NH}_3$  peak values observed during the campaign. Indeed, these emissions result from very  
35 complex mechanisms in which numerous environmental parameters are involved, including the

1 amount of nitrogen fertilizers used over the land; temperature, moisture and pH of the soil; the  
2 amount of soluble carbon; the soil disturbance and compaction; fertilization methods (Ma et al.,  
3 2010; and references therein). More elaborated parameterizations of NH<sub>3</sub> bi-directional fluxes have  
4 been proposed to better handle emission and deposition processes in CTMs (Massad et al., 2010;  
5 Zhang et al., 2010; Pleim et al., 2013). Hamaoui-Laguel et al. (2014) have simulated more realistic  
6 NH<sub>3</sub> emissions over France during the spring 2007 by combining the one-dimensional mechanistic  
7 model VOLT' AIR (Garcia et al., 2011; Générumont and Cellier, 1997) with agricultural practice and  
8 soil data. They have shown a spatial variability of NH<sub>3</sub> emissions mainly driven by the soil pH and  
9 the types and rates of fertilization, while the temporal variability was rather driven by  
10 meteorological conditions and fertilization dates. Compared to the EMEP inventory (quite similar to  
11 TNO-MP for NH<sub>3</sub> emissions), the emissions computed with the VOLT' AIR mechanism appear  
12 lower over the Brittany (in the West of France) and higher over the North of France (around a factor  
13 of 2-3). This would suggest a possible underestimation of agricultural NH<sub>3</sub> emissions close to the  
14 Paris region.

15 Dry deposition of NH<sub>3</sub> and wet deposition of NH<sub>4</sub><sup>+</sup> represent the two major sinks for NH<sub>3</sub> and  
16 NH<sub>4</sub><sup>+</sup>, respectively; the first being dominant near emission sources whereas the second dominates at  
17 a larger scale (Asman et al., 1998). Uncertainties in the parameterization of both dry and wet  
18 deposition in the CHIMERE model may also partly explain the NH<sub>3</sub> underestimation. Results from  
19 the MOD-noddep sensitivity test (with no NH<sub>3</sub> dry deposition) allow assessing an upper bound of  
20 uncertainties related to dry deposition. On average, more than half of the NH<sub>3</sub> reaching Paris is  
21 deposited in the MOD case, as illustrated by the increase of NH<sub>3</sub> concentrations by a factor of 2.2  
22 when deposition is removed. The diurnal profile indicates that deposition in CHIMERE more  
23 strongly affects night-time concentrations, likely due to the shallow boundary layer. Daytime  
24 concentrations are also affected but approximately 2 times less than night-time ones. Note that  
25 typical deposition velocities simulated by CHIMERE are around 0.3 cm s<sup>-1</sup>, although it can  
26 substantially vary in time and space. Despite the unrealistic character of this sensitivity test (dry  
27 deposition being one of the dominant NH<sub>3</sub> sinks), this appears not sufficient to increase  
28 concentrations towards observed ambient levels (NMB of -46%). Thus, deposition does not appear  
29 as the major source of error in the CHIMERE simulated NH<sub>3</sub>.

### 30 **4.2.3 Conclusions on ammonia**

31 Our NH<sub>3</sub> urban background measurements in Paris have highlighted several intense episodes in late  
32 spring and early summer. These episodes occur during anticyclonic conditions with high  
33 temperature, expected high agricultural emissions and moderate winds enabling an accumulation of  
34 NH<sub>3</sub> and a subsequent advection over the city. We argued that the observed NH<sub>3</sub> seasonal pattern

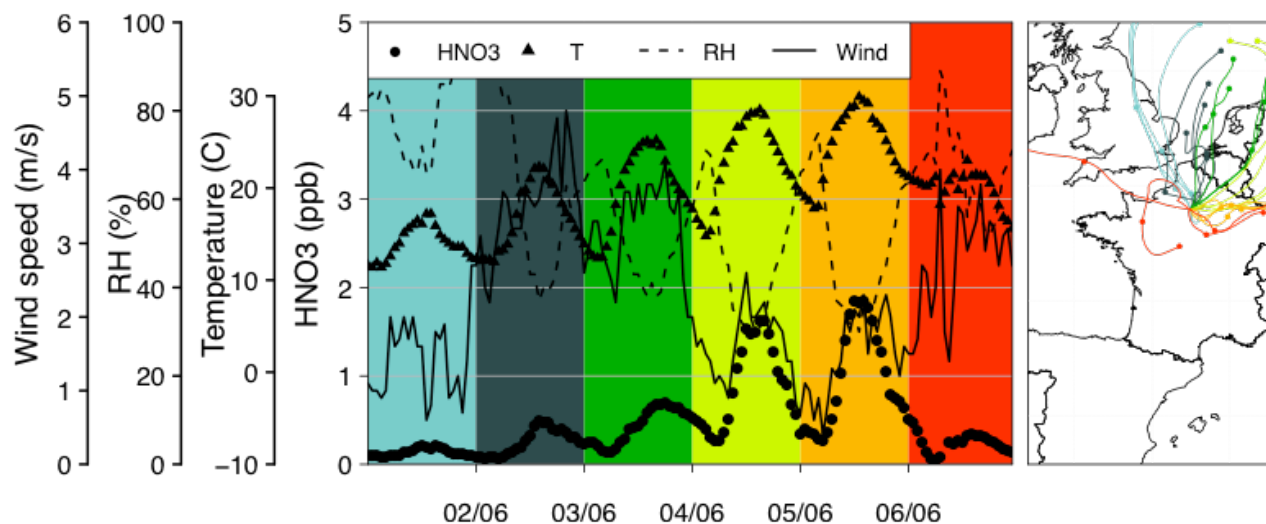
1 supports the idea of a  $\text{NH}_3$  day-to-day variability mainly driven by the agricultural source, in  
2 association with the thermodynamic equilibrium controlling the gas-aerosol partitioning.  
3 CHIMERE simulations show a significant negative bias for  $\text{NH}_3$ , both for the baseline  
4 concentrations and the intense episodes. Errors in the partitioning of  $\text{TNH}_3$  between the gas and  
5 aerosol phases (due to errors in modelled  $\text{SO}_4^{2-}$ ,  $\text{NO}_3^-$  or local meteorology) as well as uncertainties  
6 for deposition can only explain a minor part of the bias. Thus, the simulated  $\text{NH}_3$  concentrations  
7 appear mainly affected by uncertainties in emissions, and in particular the lack of dynamical  
8 treatment of agricultural emissions as a function of environmental factors (temperature, etc.) in the  
9 CHIMERE model (the annual total emissions being simply disaggregated with a monthly profile).

## 10 **4.3 Nitric acid**

### 11 **4.3.1 Temporal variability**

12 Daily concentrations and the diurnal profile of  $\text{HNO}_3$  are shown in Fig. 2. Over the whole period,  
13 the average  $\text{HNO}_3$  concentration is 0.25 ppb. Several moderate episodes are observed in spring and  
14 early summer, with daily concentrations up to 1.2 ppb at the beginning of July. This leads to a  
15 seasonal pattern characterized by higher values in spring/summer compared to autumn/winter. Such  
16 temporal variations are expected in urban environments close to  $\text{NO}_x$  emissions due to both the  
17 higher OH triggered  $\text{HNO}_3$  production in summer and the higher temperatures (as well as the lower  
18 RH) that diminish its condensation into particulate  $\text{NO}_3^-$ . They are also consistent with those found  
19 in other urban studies (Cadle et al., 1982 and Cadle, 1985 in Warren, Michigan, United-States (US);  
20 Solomon et al., 1992 in Los Angeles, California, US; Perrino et al., 2002 in Roma, Italy).

21 In Paris, the highest  $\text{HNO}_3$  episodes are associated with high temperatures and low-to-moderate  
22 wind speeds at the ground. These conditions increase the atmospheric stratification and the  
23 residence time of  $\text{NO}_x$  emissions over the agglomeration and allow for more efficient  $\text{HNO}_3$   
24 formation via the  $\text{NO}_2+\text{OH}$  reaction. This is confirmed by the fact that many  $\text{HNO}_3$  peaks follow  
25 BC episodes, these episodes often due to stagnant conditions allowing the accumulation of the BC  
26 emitted by the traffic.

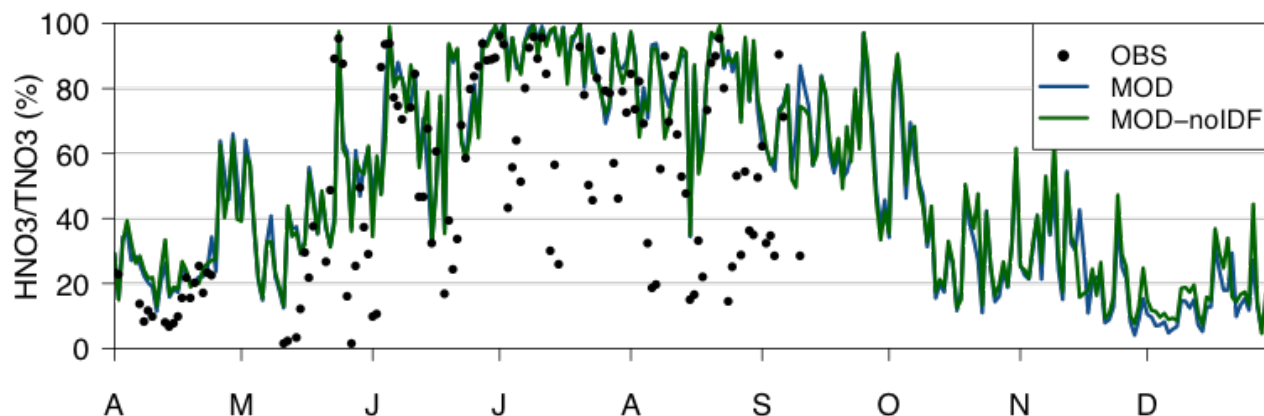


1  
 2 Figure 8: Hourly concentrations of HNO<sub>3</sub> at LHVP and wind speed, RH and temperature during  
 3 early June 2010 (left panel), and associated 48h back-trajectories (one point every 24h) coloured by  
 4 the day of arrival (i.e. red is for 06/06).

5 This is illustrated during the first days of June in Fig. 8. The 1<sup>st</sup> of June is characterized by low wind  
 6 speed but cloudy conditions that decrease the photooxidation rate of NO<sub>x</sub>. During the next 2 days,  
 7 stronger winds (above 3 m s<sup>-1</sup>) and increasing temperatures are observed, associated with a  
 8 moderate increase of HNO<sub>3</sub> concentrations. A much larger increase in HNO<sub>3</sub> concentrations is  
 9 observed on the 4<sup>th</sup> and 5<sup>th</sup> of June concomitantly with high temperatures (up to 30°C) and slow  
 10 winds. Such stagnant conditions during the night allow the accumulation of NO<sub>2</sub>, as shown by the  
 11 NO<sub>2</sub> measurements at an AIRPARIF station located right next to the LHVP site (not shown). In the  
 12 early morning of the 4<sup>th</sup> (5<sup>th</sup>) of June, NO<sub>2</sub> concentrations reach 83 (110) ppb, and fall below 20 ppb  
 13 during the afternoon. As for NH<sub>3</sub>, no additional HNO<sub>3</sub> measurements are available upwind of Paris,  
 14 which prevents us from quantitatively assessing the importance of local formation versus imports.  
 15 But this specific situation of early June supports the idea of a strong local formation of HNO<sub>3</sub>. Some  
 16 HNO<sub>3</sub> is also probably (slowly) advected by north-easterly winds but the strong photochemically  
 17 driven diurnal variation observed during these days (where concentrations reach 1.5 ppb in the  
 18 afternoon) suggests that this contribution is minor in comparison to the local formation. The episode  
 19 ends concomitantly with a significant decrease in temperature and an increase in wind speed (thus  
 20 favoring the dispersion).

21 The diurnal profile shows maximum HNO<sub>3</sub> concentrations in the afternoon at around 14:00-18:00  
 22 UTC (Fig. 2). On average, the ratio between daytime and nighttime HNO<sub>3</sub> concentrations is close to  
 23 a factor of 2 (despite the development of the convective boundary layer in the afternoon). A slight  
 24 decrease of HNO<sub>3</sub> is found at around 6:00 UTC, which may be explained by dew formation  
 25 processes that allows the absorption of water-soluble gases such as HNO<sub>3</sub> (Mulawa et al., 1986;  
 26 Parmar et al., 2001; Pierson et al., 1988) although no data are available to address this hypothesis.





1  
2 Figure 9: Daily HNO<sub>3</sub>/TNO<sub>3</sub> ratios.

3 HNO<sub>3</sub> accounts for 51% of TNO<sub>3</sub> on average (Fig. 9) but this fraction appears highly variable. The  
4 lowest HNO<sub>3</sub>/TNO<sub>3</sub> ratios (a few %) are observed during cold days in mid-May when daily  
5 temperatures fall below 8°C (see Fig. S2 in the Supplement), while the highest ratios occur during  
6 early summer, with values up to 96%. The correlation between the HNO<sub>3</sub>/TNO<sub>3</sub> ratio and the  
7 temperature is 0.82, which illustrates the impact of temperature on the thermodynamic equilibrium.  
8 Despite rather high temperatures, low ratios (below 40%) are also observed on specific periods  
9 during summer, particularly in August. Such a pattern may be due to higher measurement  
10 uncertainties occurring for low TNO<sub>3</sub> concentrations, closer to the detection limit (roughly around  
11 0.1 ppb for HNO<sub>3</sub>). In August, ratio values below 40% indeed correspond to HNO<sub>3</sub> and TNO<sub>3</sub>  
12 concentrations below 0.2 and 0.7 ppb, respectively.

### 13 4.3.2 Model results

14 HNO<sub>3</sub> concentrations are significantly overestimated by CHIMERE, with a NMB of +195% and a  
15 NRMSE of 320%, especially at mid-day when the bias can reach a factor of 4 (as illustrated by the  
16 diurnal profile in Fig. 2). The correlation is moderate ( $r=0.56$ ) when considering hourly  
17 concentrations, but is slightly higher with daily values ( $r=0.68$ ).

18 Several uncertainties may explain the discrepancies between observed and simulated HNO<sub>3</sub>  
19 concentrations: (i) uncertainties in NO<sub>x</sub> emissions at both local and regional scales, (ii) uncertainties  
20 in the thermodynamic equilibrium (i.e. the errors on either the other inorganic compounds or the  
21 ISORROPIA model itself (Fountoukis and Nenes, 2007)) that determine the distribution between  
22 gas and aerosol phases, (iii) uncertainties in the OH concentrations that directly influence the  
23 conversion of NO<sub>2</sub> into HNO<sub>3</sub>, (iv) uncertainties in the HNO<sub>3</sub> deposition, and (v) errors in the  
24 transport. At the European scale, uncertainties in NO<sub>x</sub> emissions are estimated to be around 30%  
25 (Deguillaume et al., 2007; Konovalov et al., 2006) and are thus much lower than the errors obtained  
26 for modelled HNO<sub>3</sub>. Over the Paris agglomeration, NO<sub>x</sub> emissions from the TNO-MP inventory  
27 used in our model have been evaluated during the summer 2009 based on aircraft measurements in  
28 the Paris plume, showing no significant bias (Petetin et al., 2014). Dry deposition plays an

1 important role in the HNO<sub>3</sub> budget, and corresponding parameterizations incorporated in the  
2 CHIMERE model have been poorly evaluated so far. In fact, an underestimated deposition rate in  
3 CHIMERE may partly explain the positive bias on HNO<sub>3</sub>. In CHIMERE, HNO<sub>3</sub> deposition  
4 velocities are typically below 1.5 cm s<sup>-1</sup>, which appears on the lower end of the values reported in  
5 the literature (Brook et al., 1999). However, due to a lack of appropriate data, this hypothesis  
6 remains difficult to assess. Finally, significant errors in the transport pattern remain unlikely given  
7 the good correlations obtained on nitrates between the observations and the model. The next  
8 subsections aim to investigate in more details the uncertainties related to the simulated  
9 thermodynamic equilibrium and OH radical.

#### 10 **4.3.2.1 Uncertainties associated with thermodynamic equilibrium**

11 Bias and RMSE are much lower for TNO<sub>3</sub> (NMB of +71%, NRMSE of 121%) than for HNO<sub>3</sub>,  
12 because the CHIMERE model overestimates the HNO<sub>3</sub>/TNO<sub>3</sub> fraction (on average 68% for the  
13 model against 51% observed from experimental data during the period with available observations  
14 of NO<sub>3</sub><sup>-</sup> and HNO<sub>3</sub>). Partitioning errors may derive from uncertainties in the ISORROPIA  
15 thermodynamic model (e.g. model formulation, chemical compounds included, activity coefficients  
16 treatment) or in its input data. Apart from CHIMERE, the ISORROPIA model is used in many other  
17 CTMs, including LOTOS-EUROS (Schaap et al., 2008), REM-CALGRID (Stern, 2003), CAMx,  
18 FARM or CMAQ. It has been validated in various studies based on comparisons with observations  
19 (Moya et al., 2001) or against other widely used thermodynamic models (Nenes et al., 1999;  
20 Carnevale et al., 2012). From these studies, several uncertainty sources emerge: The hypothesis  
21 (used in ISORROPIA) of an instantaneous equilibrium between gas and aerosol phases (Aan de  
22 Brugh et al., 2012) is without incidence for our study, since the CHIMERE model treats the  
23 evolution of inorganic compounds concentrations through a dynamic approach (see Sect. 3.1). The  
24 absence of sodium, chloride and other crustal species (Ca<sup>2+</sup>, K<sup>+</sup>, Mg<sup>2+</sup>) in our simulations may also  
25 induce errors in the system (Fountoukis and Nenes, 2007), but the contribution of this crustal  
26 material remains low in the Paris region, about 5% on average from 1 April to 10 September (with a  
27 percentile 95 at 13%), as previously noted by Bressi et al. (2013). This low contribution of crustal  
28 species is confirmed by the ion balance obtained when considering only ammonium, nitrate and  
29 sulfate: NH<sub>4</sub><sup>+</sup> versus NO<sub>3</sub><sup>-</sup>+2SO<sub>4</sub><sup>2-</sup> (all species expressed in ppb) gives a slope of 1.01, an y-  
30 intercept of -0.20 and a correlation r<sup>2</sup>=0.97 (see Fig. S1 in the Supplement).

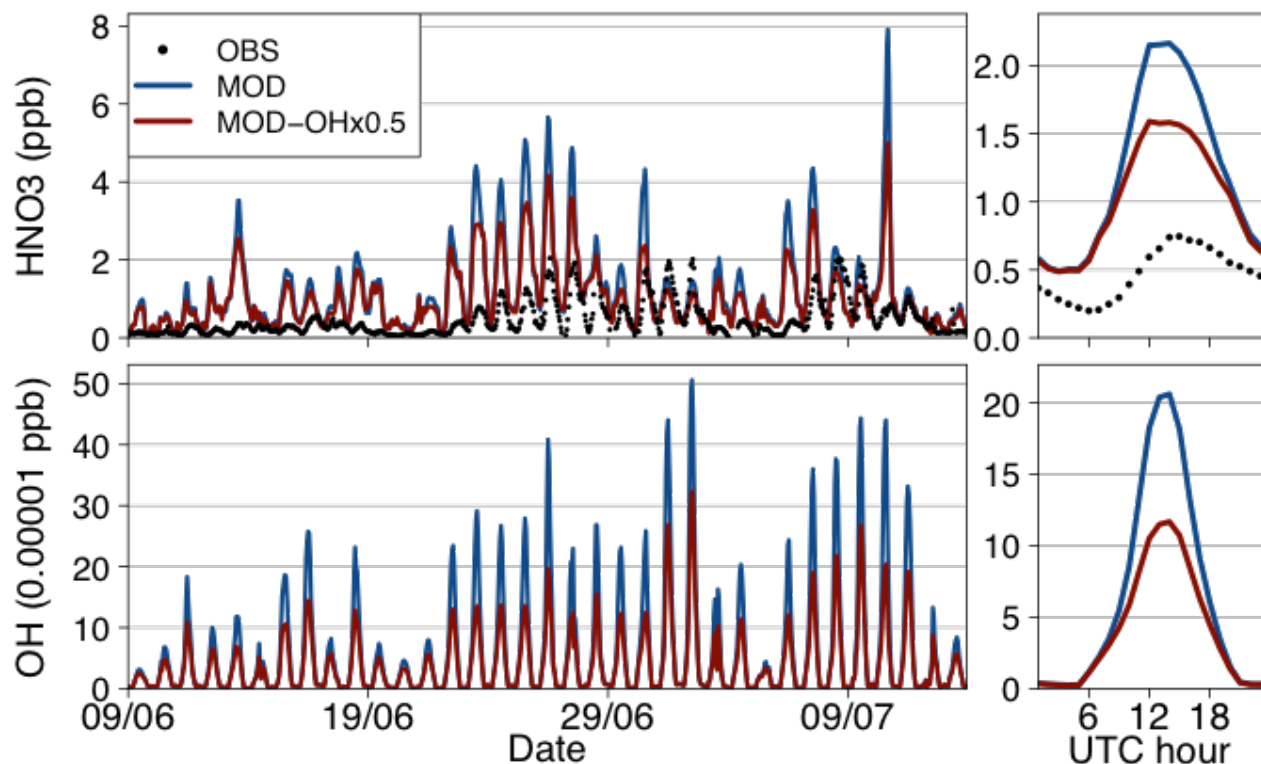
31 Therefore, errors in the modelled partitioning are most likely due to errors in the other inorganic  
32 compounds involved in the HNO<sub>3</sub>-NO<sub>3</sub><sup>-</sup> equilibrium. In particular, the large negative bias on NH<sub>3</sub>  
33 described in Sect. 4.2 can potentially lead to an underestimation of the NH<sub>4</sub>NO<sub>3</sub> formation and  
34 consequently to an overestimation of HNO<sub>3</sub>. A sensitivity test has been performed for that purpose  
35 with the ISORROPIA model running alone (i.e. not coupled with CHIMERE) fed by the

1 concentrations previously obtained with CHIMERE for inorganic species except for  $\text{NH}_3$  for which  
2 measurements were taken into account. This approach changes  $\text{HNO}_3$  concentrations, for instance a  
3 decrease of 29% in May. However, the significant positive bias in  $\text{HNO}_3$  in summer persists ( $\text{HNO}_3$   
4 concentrations decrease by only 11% between June and August), mainly because during summer  
5  $\text{NH}_4\text{NO}_3$  concentrations are very small and  $\text{HNO}_3$  is the major  $\text{TNO}_3$  component due to the  
6 relatively high temperatures.

#### 7 **4.3.2.2 Uncertainties associated with OH concentrations**

8 Assuming that (i) the  $\text{NO}_2+\text{OH}$  reaction is likely the dominant direct homogeneous pathway for  
9  $\text{HNO}_3$  formation during the summertime period, (ii) a significant bias is observed for modelled  
10  $\text{TNO}_3$ , and (iii) the maximum discrepancies between measurements and modelled  $\text{HNO}_3$  are found  
11 during mid-day, uncertainties in simulated OH could explain a substantial part of the errors on  
12  $\text{HNO}_3$ . Many studies have attempted to quantify uncertainties in sources and sinks of OH,  
13 traditionally through the direct comparison between observations and calculations from detailed  
14 chemistry schemes (in box models) fed by ancillary observations of various parameters (e.g. VOC,  
15  $\text{NO}_x$  and  $\text{O}_3$  concentrations, photolysis rates). In such exercises, uncertainties in daytime OH  
16 concentrations usually remain below a factor of 2 (see Kanaya et al. (2007) for a review, where the  
17 ratio of simulated to observed daytime OH concentrations ranges between 0.5 and 1.5). During  
18 summertime, Michoud et al. (2012) observed a very low overestimation (5%) of simulated OH  
19 concentrations in Paris using the Master Chemical Mechanism (MCM) chemistry scheme.  
20 However, these results need to be taken as a lower end of OH uncertainties in CTMs where  
21 constraints are neither applied on long-lived compounds nor on photolysis rates. This is especially  
22 true in an urban environment where concentration gradients of compounds impacting on the OH  
23 budget are strong.

24 In order to assess the influence of OH on  $\text{HNO}_3$  formation, a sensitivity test (hereafter designated  
25 by MOD-OHx0.5) has been performed over a period of 35 days in June/early July by artificially  
26 reducing OH concentrations. This is technically performed by decreasing by a factor of 2 the  $\text{HO}_x$   
27 ( $\text{HO}_x=\text{OH}+\text{HO}_2+\text{RO}_2$ ) formation yields (i.e. the stoichiometric coefficient) in several (initiation)  
28 reactions, including the photolytic destruction of  $\text{O}_3$ , formaldehyde, acetaldehyde, glyoxal and  
29 methyl glyoxal. OH and  $\text{HNO}_3$  concentrations are then compared to the reference MOD case in Fig.  
30 10. On average, concentrations of OH and  $\text{HNO}_3$  are reduced by -36 and -16%, respectively. The  
31 changes in  $\text{NO}_x$  concentrations remain below 3%, which means that only a minor fraction of  $\text{NO}_x$  is  
32 oxidized within Paris. These decreases are even larger during mid-day when they reach -42 and -  
33 25%, respectively. Over mid-day, the bias between measured and modelled  $\text{HNO}_3$  is reduced to  
34 +113% (compared to +154% in the MOD case). Uncertainties in the OH radical may thus explain a  
35 significant part of the CHIMERE errors on  $\text{HNO}_3$ .



1  
 2 Figure 10: HNO<sub>3</sub> and OH hourly concentrations (left panel) and diurnal profiles (right panel) at the  
 3 LHVP site.

#### 4 4.3.3 Conclusions on HNO<sub>3</sub>

5 HNO<sub>3</sub> concentrations experimentally determined in Paris show several intense peaks in late spring  
 6 and early summer that coincide with high air temperatures and low to moderate wind speeds. The  
 7 share between local production and imports remains difficult to assess precisely, but local HNO<sub>3</sub>  
 8 may represent a major source during some specific time-limited episodes. However, uncertainties  
 9 persist, and the CHIMERE errors are unfortunately too high to help the investigation of HNO<sub>3</sub>  
 10 origin. Indeed, the model largely overestimates measured HNO<sub>3</sub> concentrations, approximately by a  
 11 factor 3, with the highest biases observed in the middle of the day. The negative bias between  
 12 measured and modelled NH<sub>3</sub> explains a part of the poor model performance for HNO<sub>3</sub>, but still fails  
 13 to explain errors during summertime when TNO<sub>3</sub> is mostly in the gas phase. Uncertainties in NO<sub>x</sub>  
 14 emissions are much lower than errors obtained on HNO<sub>3</sub> and cannot explain the results of the  
 15 model. Uncertainties related to the dry deposition of HNO<sub>3</sub> cannot be assessed and could contribute  
 16 to the discrepancies given by the model. Finally, a too large NO<sub>2</sub>-to-HNO<sub>3</sub> conversion through an  
 17 overestimation of the OH radical concentrations in CHIMERE could also contribute to the large  
 18 modelled overestimation of HNO<sub>3</sub> formation. Indeed, due to the absence of appropriate validation,  
 19 uncertainties in simulated OH still remain high in CHIMERE (probably more than a factor of 2) and  
 20 reducing OH sources have shown to lead to a significant decrease in OH and HNO<sub>3</sub> concentrations,  
 21 in particular during the afternoon when NO<sub>2</sub> photooxidation (as well as the HNO<sub>3</sub> bias) is at its  
 22 maximum.

## 1 4.4 Aerosol Nitrate formation

### 2 4.4.1 Results of the CHIMERE simulations

3 Fine particulate pollution with high  $\text{NO}_3^-$  contents in Paris consists of intense (up to  $16 \mu\text{g m}^{-3}$  in  
4 late spring) and time-limited (a few days) episodes associated with continental wind regimes. Very  
5 low levels of nitrate are observed during periods with marine (clean) air masses and during  
6 summertime (due to volatilization). Despite the large errors previously highlighted for both  $\text{NH}_3$   
7 and  $\text{HNO}_3$ , the CHIMERE model provides relatively good results for nitrate with a NMB of +19%  
8 and a correlation of 0.81, but still with a large NRMSE (109%). As previously mentioned, in the  
9 framework of the PARTICULES campaign,  $\text{PM}_{2.5}$  chemical constituents have also been measured  
10 at three rural sites around the Paris region. Results have been analyzed in terms of local and  
11 imported contributions by Petetin et al. (2014) who found that imported sulfate was slightly  
12 underestimated by CHIMERE (-17%) while the local production of sulfate was overestimated  
13 (+32%), leading at the end to a moderate negative bias (-17%). For nitrates, they found a similar but  
14 larger error compensation identified between imported and local production (bias of +63 and -  
15 109%, respectively), leading to a bias in Paris of +23%. More details can be found in Petetin et al.  
16 (2014) (e.g. statistical results in Table 7).

17 It is worth noting that the positive bias highlighted here on the urban background concentrations in  
18 Paris should partly originate from experimental (negative) artifacts. The model may underestimate  
19  $\text{NO}_3^-$  if the experimental data are corrected for semi-volatile losses. The semi-volatile particulate  
20 matter (SVPM) can be deduced from the difference between TEOM-FDMS and TEOM  $\text{PM}_{2.5}$   
21 concentrations. If we attribute all that SVPM to  $\text{NH}_4\text{NO}_3$ , the bias between measured and modelled  
22  $\text{NO}_3^-$  becomes -48%. This corresponds to an upper bound of the bias since SVPM not only contains  
23  $\text{NH}_4\text{NO}_3$  but also semi-volatile OA. Semi-volatile OA may contribute the most to SVPM, as  
24 suggested by the higher correlation of SVPM with OA in comparison with  $\text{NH}_4\text{NO}_3$  (0.59 versus  
25 0.32).

26 As a conclusion, the either positive or negative bias in simulated nitrates and ammonium remains  
27 relatively small in comparison with the biases reported previously for precursor species. Such a  
28 result is not intuitive, and cannot be trivially explained. An interesting point to illustrate is the  
29 possible error compensation related to the saturation condition that needs to be achieved to allow  
30 the formation of nitrates. This condition is defined as (Ansari and Pandis, 1998):

$$31 \quad [T\text{NO}_3]([T\text{NH}_3] - 2[T\text{S}]) > K \quad (6)$$

32 with K being the equilibrium constant that depends on various parameters, including temperature  
33 and RH. It is obvious here that the errors in  $T\text{NO}_3$  and  $T\text{NH}_3$  can partly compensate each other. On  
34 average, the left-hand term is 3.6 and 2.5  $\text{ppb}^2$  based on observations and simulation, respectively,  
35 which corresponds to a NMB of -31%, thus much lower than the NMB affecting the different

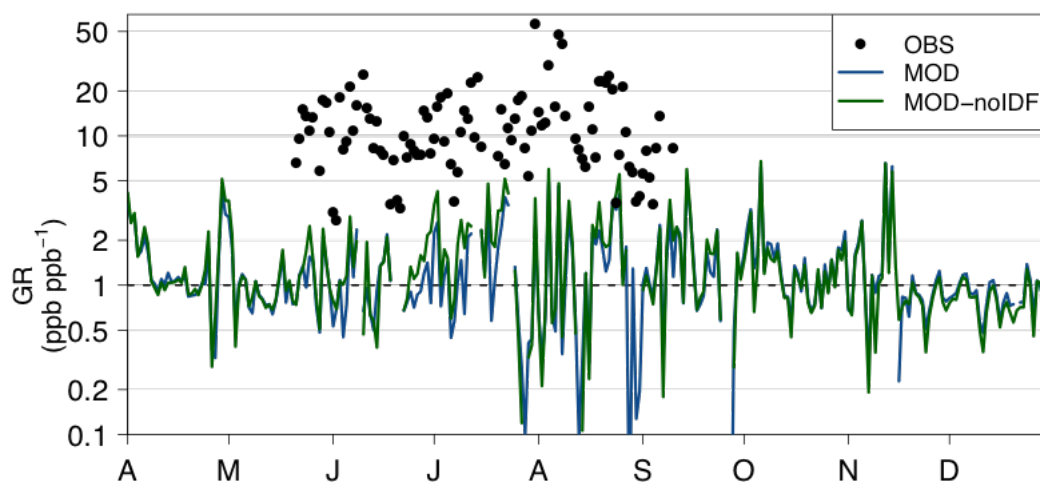
1 species (+71%, -56% and +48% for  $TNO_3$ ,  $TNH_3$  and TS). This result thus suggests that the  
 2 formation of nitrates is slightly less thermodynamically favored in the model than in the reality,  
 3 which would be consistent with a moderate negative bias in nitrates. Due to possible artefacts, our  
 4 dataset does not allow a complete assessment of the nitrate formation. It would be useful in the near  
 5 future to evaluate the CHIMERE model with artefact-free measurements (for instance with aerosol  
 6 mass spectrometer (AMS) or aerosol chemical speciation monitor (ACSM)).

#### 7 4.4.2 Gas Ratio and limiting species for nitrate formation

8 The Gas Ratio (GR) has been proposed to assess which species among  $NH_3$  and  $HNO_3$  is the  
 9 limiting reactant for  $NH_4NO_3$  formation (Ansari and Pandis, 1998). It is defined as follows (with  
 10 concentrations expressed in ppb):

$$11 \quad GR = \frac{[TNH_3] - 2[TS]}{[TNO_3]} \quad (7)$$

12 GR values above 1 indicate a regime mainly limited by  $HNO_3$  (i.e.  $NH_3$ -rich regime) in which there  
 13 is enough  $NH_3$  to neutralize both sulfate and nitrate. Conversely, a GR between 0 and 1 indicates  
 14 that there is enough  $NH_3$  to neutralize sulfate but not nitrate, while negative GR corresponds to a  
 15  $NH_3$ -poor regime in which  $NH_3$  amounts are insufficient to even neutralize sulfate. Non-linear PM  
 16 responses to inorganic concentration changes are expected at GR near unity (Ansari and Pandis,  
 17 1998).



18  
 19 Figure 12: Observed and modelled daily GR.

20 As shown on Fig. 12, daily GR measurements are available only from the end of May (no  $NH_3$   
 21 observations before) until the beginning of September (no aerosol observations after). During that  
 22 period, experimentally determined daily GR values are highly variable (ranging between 2.8 to  
 23 56.3) but always remain above unity (12.6 on average), thus indicating that a large amount of  
 24 ammonia is available for neutralizing nitric acid.

25 Observed GR may be affected by negative artefacts of nitrate filter measurements (Sect. 2.1). If we  
 26 assume here that all the SVPM is  $NH_4NO_3$  (see Sect. 4.4.1), one can calculate an artefact-corrected

1 GR with both evaporated  $\text{NH}_4^+$  and  $\text{NO}_3^-$  added to measured  $\text{TNH}_3$  and  $\text{TNO}_3$ , respectively.  
2 Compared to the previous GR, the artefact-corrected GR is reduced to an average value of 7.3 (the  
3 median is 3.5), thus still well above 1. In addition, as noticeable amounts of OA is expected to be  
4 included in the evaporated portion, this artefact-corrected GR has to be considered as a lower  
5 estimate of the actual GR values. The nitrate formation in Paris thus appears mainly limited by  
6  $\text{HNO}_3$ . Over Europe, Pay et al. (2012) have also observed GR above 1 in several regions (e.g.  
7 Switzerland, Italy, Austria, inland regions of Spain and Denmark; no data in France), but taking into  
8 account observations restricted to regional background stations (i.e. enriched by agriculture ( $\text{NH}_3$ )  
9 emissions instead of traffic ( $\text{NO}_x$ ) emissions). In our study, we show that such a  $\text{NH}_3$ -rich regime is  
10 also observed within a large megacity like Paris. Considering the high  $\text{NO}_x$  emissions in the Paris  
11 megacity, such a result is counter-intuitive, but may be explained (as previously mentioned in Sect.  
12 4.3.2) by a too slow  $\text{NO}_x$ -to- $\text{HNO}_3$  conversion rate compared to the efficient dispersive conditions.  
13 In the CHIMERE model, the negative bias for  $\text{TNH}_3$  and the positive biases for  $\text{TNO}_3$  and  $\text{SO}_4^{2-}$   
14 result in a significant underestimation of modelled GR. On average, the model simulates a GR  
15 slightly above unity (1.2). Daily values continuously alternate between the  $\text{NH}_3$ -rich and  $\text{NH}_3$ -poor  
16 regimes with 48% of simulated daily values remaining below unity (47% considering the whole  
17 dataset). The diurnal profile given by CHIMERE indicates that the GR regime changes within a  
18 single day, the lowest GR values (below 1) being simulated at 12:00 UTC (between the maximum  
19  $\text{TNO}_3$  occurring at 8:00 UTC and the minimum  $\text{TNH}_3$  simulated at 15:00 UTC). Therefore, due to  
20 significant errors in gaseous precursors (and to a lesser extent in sulfate), the CHIMERE model fails  
21 half of time at correctly simulating the  $\text{HNO}_3$ -limited regime for nitrate formation in Paris on a  
22 daily basis.

### 23 4.4.3 Sensitivity to perturbations

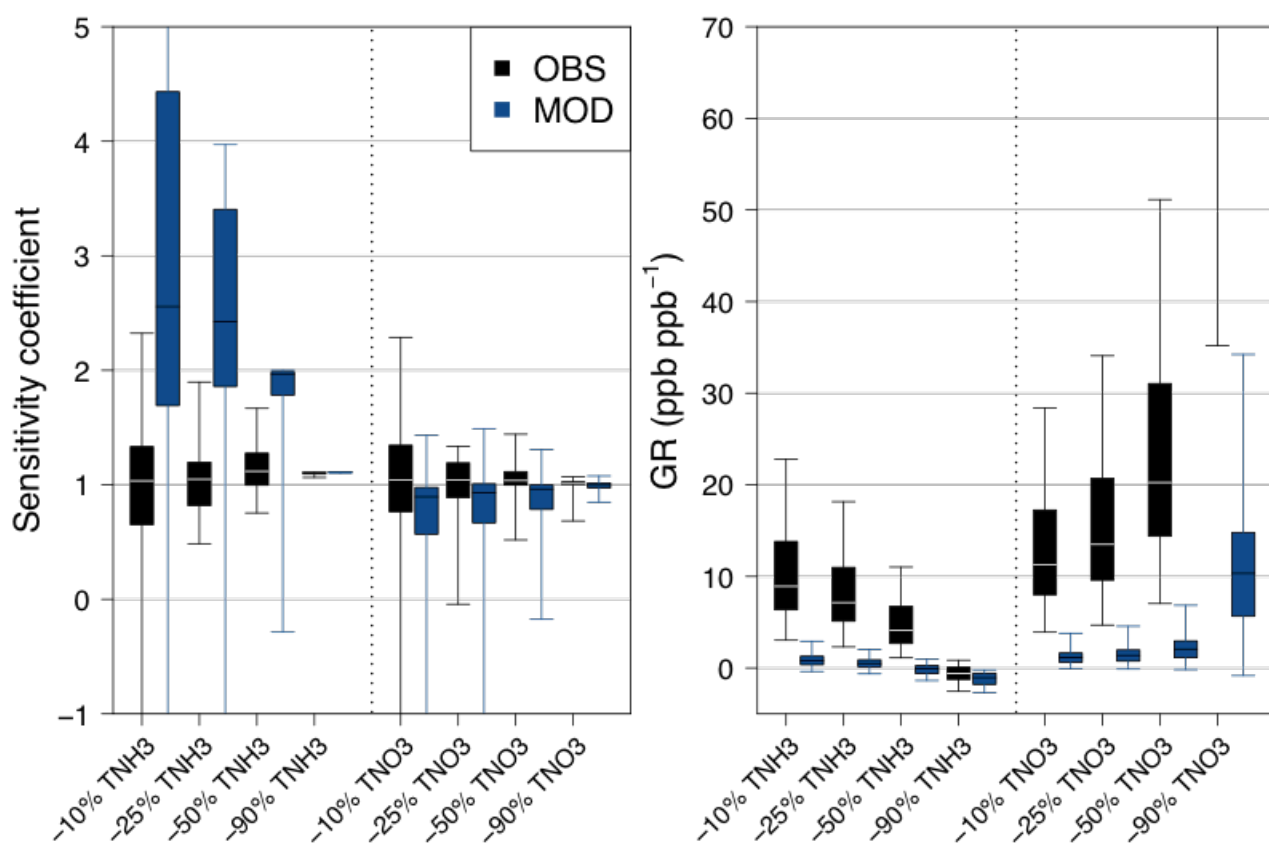
24 The GR value alone does not allow predicting the sensitivity of nitrate formation with respect to  
25 changes in gas precursor concentrations. This is due to the inability of GR to take into account both  
26 the need for the atmosphere to be saturated with  $\text{NH}_3$  and  $\text{HNO}_3$  (which acts as a threshold effect,  
27 see formula 6 in Sect. 4.4.1), and the influence of temperature and RH. Additional information can  
28 be given by the sensitivity coefficient  $S_x$  (Takahama et al., 2004) of nitrate formation, defined as:

$$29 \quad S_x = \frac{\Delta \text{NO}_3}{\text{NO}_3} \frac{x}{\Delta x} \quad (8)$$

30 where  $\Delta \text{NO}_3$  refers to the change in nitrate concentrations obtained after a  $\Delta x$  change of the  
31 parameter  $x$  (e.g. temperature, RH,  $\text{TNH}_3$ ,  $\text{TNO}_3$  or TS).

32 The ISORROPIA thermodynamic model is used here to compute the sensitivity coefficient  $S_x$  as a  
33 function of various decreases (-10, -25, -50 and -90%) in  $\text{TNH}_3$  and  $\text{TNO}_3$  concentrations. This 0-  
34 dimension model requires five inputs – temperature, RH, and  $\text{TNO}_3$ ,  $\text{TNH}_3$  and TS concentrations  
35 – and computes the gas-aerosol partitioning coefficient for  $\text{TNO}_3$  and  $\text{TNH}_3$  compounds. Also note

1 that the analysis is local, as it is performed for the observed and simulated set of parameters at the  
 2 urban background site. Decreasing the concentration of  $\text{TNO}_3$  (or  $\text{TNH}_3$ ) leads to a change in its  
 3 partitioning between both the gas and aerosol phases. This change not only depends on the  
 4 concentration of the family species which is altered but also on the value of all the other parameters  
 5 of the system. Thus, the CHIMERE errors in the different input parameters propagate to the gas-  
 6 aerosol partitioning coefficient, which can potentially lead to an erroneous sensitivity of nitrates to a  
 7 change in  $\text{TNO}_3$  or  $\text{TNH}_3$ . Calculations are performed for both the measurements and the model, i.e.  
 8 all inputs are taken from the observations and the model, respectively, at the urban background site.  
 9 In each case, the (observed or simulated) concentrations of  $\text{TNH}_3$  or  $\text{TNO}_3$  are decreased and the  
 10 sensitivity coefficient is computed to quantify the impact of this change on the nitrate  
 11 concentrations. Sensitivity coefficient results and corresponding GR are shown in Fig. 13.



12  
 13 Figure 13: Sensitivity coefficient  $S_x$  of nitrate formation due to different changes (-10, -25, -50 and  
 14 90%) in  $\text{TNH}_3$  and  $\text{TNO}_3$  concentrations (left panel) and resulting GR (right panel) during the  
 15 period from 15 May to 10 September 2010. Experimental data (OBS) in black, modelled data  
 16 (MOD) in blue. Box plots indicate 5<sup>th</sup>, 25<sup>th</sup>, 50<sup>th</sup>, 75<sup>th</sup> and 95<sup>th</sup> percentiles.

17 For the experimental data, we do observe a quite similar sensitivity of nitrate formation for changes  
 18 either in  $\text{TNH}_3$  or in  $\text{TNO}_3$  concentrations, with median sensitivity coefficients around 1 (i.e. close  
 19 to a linear response). Considering the high GR values (except for the -50 and -90%  $\text{TNH}_3$  cases that  
 20 lead to negative GR), such a result with similar responses to both precursors changes appears quite  
 21 counter-intuitive in light of the above definition of GR. However, first, the GR approach considers



1 free  $\text{NH}_3$ , while the sensitivities are calculated with respect to total  $\text{NH}_3$ . Second, as already  
2 mentioned, the formation of nitrates requires the saturation condition to be achieved (see formula  
3 6). So for large GR values, but small  $\text{TNO}_3$  and free  $\text{NH}_3$  values, nitrate formation will be sensitive  
4 to both  $\text{TNO}_3$  and  $\text{TNH}_3$ . Note that the equilibrium constant K (and thus the nitrate sensitivity) also  
5 depends on temperature and RH; this is illustrated in Fig. S6 in the Supplement where the same  
6 sensitivity tests are performed after decreasing the temperature by  $10^\circ\text{C}$  and increasing the RH by  
7 0.20 in observations, which leads to  $S_{\text{TNO}_3}$  (still close to 1) much higher than  $S_{\text{TNH}_3}$  (below 0.5 for -  
8 10 and -25% of  $\text{TNH}_3$ ), in accordance with the  $\text{NH}_3$ -rich regime given by GR.

9 The CHIMERE nitrate response to  $\text{TNO}_3$  changes is approximately linear (i.e.  $S_{\text{TNO}_3}$  close to 1), in  
10 reasonable agreement with observations. However, the model highly overestimates the sensitivity to  
11  $\text{TNH}_3$  changes, with median  $S_{\text{TNH}_3}$  up to 2.5 for moderate  $\text{NH}_3$  decreases while observations show  
12 (as for  $\text{TNO}_3$  changes) a linear response to  $\text{TNH}_3$  changes (i.e.  $S_{\text{TNH}_3}$  around 1). The model is able  
13 to reproduce the observed response only when  $\text{NO}_3^-$  formation is severely  $\text{NH}_3$ -limited (negative  
14 GR) and when the aerosol nitrate formation is prevented (which corresponds to the -90%  $\text{TNH}_3$   
15 case).

16 These results have serious implications on the use of the CHIMERE model for emissions reduction  
17 scenarios. As  $\text{TNH}_3$  concentrations are closely linked to  $\text{NH}_3$  emissions, they show that the benefits  
18 (in terms of fine aerosol concentrations) of reducing these emissions would likely be overestimated  
19 by the model, in particular for moderate reductions (below -50%). In addition, in terms of  
20 dynamical evaluation, changes in  $\text{NH}_3$  emissions in the next years may potentially degrade the  
21 CHIMERE performance on the simulation of  $\text{NH}_4\text{NO}_3$  in Paris if the issues raised here are not  
22 addressed. This is an important conclusion for the use of the CHIMERE model (in that  
23 configuration and input data).

24

## 25 **5 Conclusions**

26 Ammonium nitrate is a major contributor to the fine particulate pollution in Europe, and a better  
27 characterization of its formation regime and variability (controlled by the availability of its gaseous  
28 precursors,  $\text{NH}_3$  and  $\text{HNO}_3$ ) is thus mandatory for setting up relevant PM control strategies.

29 In this study, long term measurements of inorganic compounds in both gaseous ( $\text{NH}_3$ ,  $\text{HNO}_3$ ,  $\text{SO}_2$ )  
30 and aerosol ( $\text{NH}_4^+$ ,  $\text{NO}_3^-$ ,  $\text{SO}_4^{2-}$ ) fractions have been used to assess the  $\text{NO}_3^-$  formation regime in the  
31 Paris megacity over several months covering the spring/summer period of 2010. High episodes of  
32  $\text{NH}_3$  (up to 12 ppb on daily average) were observed during late spring and early summer.  
33 Considering both the seasonal and diurnal variations, these observations suggest that agricultural  
34 activities are a major driver of the  $\text{NH}_3$  day-to-day variability within the Paris megacity. Rather low  
35  $\text{HNO}_3$  concentrations were measured (below 1.5 ppb on daily average), despite the large amounts of

1 gas precursors ( $\text{NO}_x$ ) emitted by the traffic in the city of Paris. Some elevated  $\text{HNO}_3$  episodes were  
2 observed during anticyclonic conditions (high temperature, low-to-moderate wind) and suggest a  
3 substantial local formation from the  $\text{NO}_x$  emitted within Paris. However, our dataset does not allow  
4 quantitatively assessing the relative contributions of this local formation as compared to imports.  
5 These experimental results lead to a  $\text{NH}_3$ -rich regime in the Paris urban environment (as indicated  
6 by high GR values), as already observed in previous studies over Europe but only in rural areas (i.e.  
7 closer to agricultural activities). However, sensitivity tests with the ISORROPIA thermodynamic  
8 model indicate that, in the specific environment of Paris (in terms of RH, temperature and inorganic  
9 compounds concentrations), the  $\text{NO}_3^-$  formation remains equally influenced by decreases of  $\text{TNH}_3$   
10 and  $\text{TNO}_3$ . Considering the size of the Paris megacity and the intensity of  $\text{NO}_x$  emissions, one  
11 would have primarily expected higher  $\text{HNO}_3$  and lower  $\text{NH}_3$  in the Paris center. This work thus  
12 sheds a new light on the topical debate relative to the respective responsibility of traffic and  
13 agriculture in the formation of  $\text{NH}_4\text{NO}_3$ , by highlighting substantial amounts of agricultural  $\text{NH}_3$   
14 and relatively low concentrations of  $\text{HNO}_3$  in the city.

15 This detailed experimental dataset has also offered the opportunity to evaluate for the first time the  
16 ability of the CHIMERE chemistry-transport model to simulate the  $\text{NH}_3$ - $\text{HNO}_3$ - $\text{NO}_3^-$  system.  
17 Comparison between measurements and model estimates have shown significant negative (-75%)  
18 and positive (+195%) biases for  $\text{NH}_3$  and  $\text{HNO}_3$ , respectively. Several sensitivity tests have been  
19 performed in order to rank the uncertainty sources responsible for these biases. The difficulty of the  
20 CHIMERE model to match  $\text{NH}_3$  observations is likely due primarily to erroneous agricultural  
21 emissions (in particular their spatio-temporal variability). By comparison, the contribution of  $\text{NH}_3$   
22 traffic emissions in the Paris agglomeration appears minor during the studied period but requires a  
23 more detailed quantification. Besides the (hardly quantifiable) uncertainties associated with dry  
24 deposition, errors in  $\text{HNO}_3$  can probably be explained by the large uncertainties in OH  
25 concentrations, in particular during summertime, while the negative bias in  $\text{NH}_3$  explains a  
26 noticeable portion of the  $\text{HNO}_3$  overestimation during spring (by preventing  $\text{HNO}_3$  conversion to  
27  $\text{NO}_3^-$ ).

28 The sensitivity of  $\text{NO}_3^-$  formation as a function of decreasing concentrations of gas precursor have  
29 been investigated, highlighting a very high sensitivity to  $\text{NH}_3$  changes in the model, in disagreement  
30 with observations that give a quasi linear response. Such results may have important implications  
31 on the use of CHIMERE for emission reduction scenarios (at least in the Paris region) by potentially  
32 overestimating the benefit of  $\text{NH}_3$  emission reductions in terms of reductions of PM concentrations.  
33 The diagnostic evaluation led in this paper gives first results that need to be extended, notably with  
34 hourly artefact-free ( $\text{NH}_4\text{NO}_3$ ) measurements during all seasons, in order to assess more precisely  
35 the  $\text{NO}_3^-$  formation regime in the city of Paris. Additional work on uncertainty sources is also

1 required to reduce the highlighted errors, in particular the NH<sub>3</sub> agricultural emissions and the OH  
2 uncertainties. The recent NH<sub>3</sub> measurements provided by IASI (Infrared Atmospheric Sounding  
3 Interferometer; Clarisse et al., 2009, 2010) may offer opportunities to better assess the spatial  
4 distribution of NH<sub>3</sub> emissions and help build more accurate emission inventories.

5

## 6 **Acknowledgements**

7 This work is funded by a PhD DIM (*domaine d'intérêt majeur*) grant from the Ile-de-France region.  
8 The PARTICULES project has been funded by the French state, the Ile-de-France region and the  
9 Paris city. The FRANCIPOL projet has received funding from PRIMEQUAL, CNRS, CEA, the Ile-  
10 de-France region, ACTRIS and DIM R2DS. The authors gratefully acknowledge Jean-Charles  
11 Dupont and the SIRTA ([sirta.ipsl.fr](http://sirta.ipsl.fr)) for the useful boundary layer height data. The other  
12 meteorological data at Montsouris site have been kindly provided by METEO France.

## 13 **References**

- 14 Aan de Brugh, J. M. J., Henzing, J. S., Schaap, M., Morgan, W. T., van Heerwaarden, C. C., Weijers,  
15 E. P., Coe, H. and Krol, M. C.: Modelling the partitioning of ammonium nitrate in the convective  
16 boundary layer, *Atmos. Chem. Phys.*, 12(6), 3005–3023, doi:10.5194/acp-12-3005-2012,  
17 2012.
- 18 Airparif: Inventaire des émissions en Ile-de-France en 2005., 2010.
- 19 Airparif: Origine des particules en Ile-de-France., 2011.
- 20 Airparif: Source apportionment of airborne particles in the Ile-de-France region., 2012.
- 21 Ansari, A. S. and Pandis, S. N.: Response of Inorganic PM to Precursor Concentrations, *Environ.*  
22 *Sci. Technol.*, 32(18), 2706–2714, doi:10.1021/es971130j, 1998.
- 23 Asman, W. A. H., Sutton, M. A. and Schjorring, J. K.: Ammonia: emission, atmospheric transport  
24 and deposition, *New Phytol.*, 139(1), 27–48, doi:10.1046/j.1469-8137.1998.00180.x, 1998.
- 25 Baklanov, A., Lawrence, M., Pandis, S., Mahura, A., Finardi, S., Moussiopoulos, N., Beekmann, M.,  
26 Laj, P., Gomes, L., Jaffrezo, J.-L., Borbon, A., Coll, I., Gros, V., Sciare, J., Kukkonen, J., Galmarini, S.,  
27 Giorgi, F., Grimmond, S., Esau, I., Stohl, A., Denby, B., Wagner, T., Butler, T., Baltensperger, U.,  
28 Builtjes, P., van den Hout, D., van der Gon, H. D., Collins, B., Schlunzen, H., Kulmala, M.,  
29 Zilitinkevich, S., Sokhi, R., Friedrich, R., Theloke, J., Kummer, U., Jalkinen, L., Halenka, T.,  
30 Wiedensholer, A., Pyle, J. and Rossow, W. B.: MEGAPOLI: concept of multi-scale modelling of  
31 megacity impact on air quality and climate, *Adv. Sci. Res.*, 4, 115–120, doi:10.5194/asr-4-115-  
32 2010, 2010.
- 33 Bessagnet, B., Menut, L., Curci, G., Hodzic, A., Guillaume, B., Liousse, C., Moukhtar, S., Pun, B.,  
34 Seigneur, C. and Schulz, M.: Regional modeling of carbonaceous aerosols over Europe - focus  
35 on secondary organic aerosols, *J. Atmos. Chem.*, 61(3), 175–202, doi:10.1007/s10874-009-  
36 9129-2, 2009.
- 37 Bishop, G. A., Peddle, A. M., Stedman, D. H. and Zhan, T.: On-road emission measurements of  
38 reactive nitrogen compounds from three California cities., *Environ. Sci. Technol.*, 44(9), 3616–  
39 20, doi:10.1021/es903722p, 2010.
- 40 Blanchard, C. L. and Hidy, G. M.: Effects of changes in sulfate, ammonia, and nitric acid on  
41 particulate nitrate concentrations in the Southeastern United States, *J. Air Waste Manage.*  
42 *Assoc.*, 53(3), 283–290, doi:10.1080/10473289.2003.10466152, 2003.
- 43 Bressi, M., Sciare, J., Gherzi, V., Bonnaire, N., Nicolas, J. B., Petit, J.-E., Moukhtar, S., Rosso, A.,

1 Mihalopoulos, N. and Féron, A.: A one-year comprehensive chemical characterisation of fine  
2 aerosol (PM<sub>2.5</sub>) at urban, suburban and rural background sites in the region of Paris (France),  
3 *Atmos. Chem. Phys.*, 13(15), 7825–7844, doi:10.5194/acp-13-7825-2013, 2013.

4 Brook, J. R., Zhang, L., Li, Y. and Johnson, D.: Description and evaluation of a model of  
5 deposition velocities for routine estimates of dry deposition over North America. Part II:  
6 review of past measurements and model results, *Atmos. Environ.*, 33(30), 5053–5070,  
7 doi:10.1016/S1352-2310(99)00251-4, 1999.

8 Cadle, S. ., Countess, R. . and Kelly, N. .: Nitric acid and ammonia in urban and rural locations,  
9 *Atmos. Environ.*, 16(10), 2501–2506, doi:10.1016/0004-6981(82)90141-X, 1982.

10 Cadle, S. H.: Seasonal variations in nitric acid, nitrate, strong aerosol acidity, and ammonia in  
11 an urban area, *Atmos. Environ.*, 19(1), 181–188, doi:10.1016/0004-6981(85)90149-0, 1985.

12 Camargo, J. A. and Alonso, A.: Ecological and toxicological effects of inorganic nitrogen  
13 pollution in aquatic ecosystems: A global assessment., *Environ. Int.*, 32(6), 831–49,  
14 doi:10.1016/j.envint.2006.05.002, 2006.

15 Carnevale, C., Finzi, G., Pisoni, E., Thunis, P. and Volta, M.: The impact of thermodynamic  
16 module in the CTM performances, *Atmos. Environ.*, 61, 652–660,  
17 doi:10.1016/j.atmosenv.2012.06.058, 2012.

18 Carslaw, D. C. and Rhys-Tyler, G.: New insights from comprehensive on-road measurements of  
19 NO<sub>x</sub>, NO<sub>2</sub> and NH<sub>3</sub> from vehicle emission remote sensing in London, UK, *Atmos. Environ.*, 81,  
20 339–347, doi:10.1016/j.atmosenv.2013.09.026, 2013.

21 Chow, J. C.: Health Effects of Fine Particulate Air Pollution: Lines that Connect, *J. Air Waste*  
22 *Manage. Assoc.*, 56(6), 707–708, doi:10.1080/10473289.2006.10464484, 2006.

23 CITEPA: Inventaire des émissions de polluants atmosphériques et de gaz à effet de serre en  
24 France - Séries sectorielles et analyses étendues., 2013.

25 Clarisse, L., Clerbaux, C., Dentener, F., Hurtmans, D. and Coheur, P.-F.: Global ammonia  
26 distribution derived from infrared satellite observations, *Nat. Geosci.*, 2(7), 479–483,  
27 doi:10.1038/ngeo551, 2009.

28 Clarisse, L., Shephard, M. W., Dentener, F., Hurtmans, D., Cady-Pereira, K., Karagulian, F., Van  
29 Damme, M., Clerbaux, C. and Coheur, P.-F.: Satellite monitoring of ammonia: A case study of  
30 the San Joaquin Valley, *J. Geophys. Res.*, 115(D13302), doi:10.1029/2009JD013291, 2010.

31 Dall'Osto, M., Harrison, R. M., Coe, H. and Williams, P.: Real-time secondary aerosol formation  
32 during a fog event in London, *Atmos. Chem. Phys.*, 9(7), 2459–2469, doi:10.5194/acp-9-2459-  
33 2009, 2009.

34 Davidson, C. I. and Wu, Y. L.: Dry deposition of particle and vapors, in S. E. Lindberg, A. L. Page  
35 and S. A. Norton (ads.): *Acidic precipitation* (vol. 3). Springer Verlag, New York, pp. 103–216.,  
36 1990.

37 Deguillaume, L., Beekmann, M. and Menut, L.: Bayesian Monte Carlo analysis applied to  
38 regional-scale inverse emission modeling for reactive trace gases, *J. Geophys. Res.*,  
39 112(D02307), doi:10.1029/2006JD007518, 2007.

40 Development, U., Kuenen, J., Gon, H. D. Van Der, Visschedijk, A. and Brugh, V. Der: MACC  
41 European emission inventory for the years 2003-2007, 2011.

42 Erisman, J. W., Van Pul, A. and Wyers, P.: Parametrization of surface resistance for the  
43 quantification of atmospheric deposition of acidifying pollutants and ozone, *Atmos. Environ.*,  
44 28(16), 2595–2607, doi:10.1016/1352-2310(94)90433-2, 1994.

45 Erisman, J. W., Otjes, R., Hensen, A., Jongejan, P., van den Bulk, P., Khlystov, A., Möls, H. and  
46 Slanina, S.: Instrument development and application in studies and monitoring of ambient  
47 ammonia, *Atmos. Environ.*, 35(11), 1913–1922, doi:10.1016/S1352-2310(00)00544-6, 2001.

48 Flechard, C. R., Nemitz, E., Smith, R. I., Fowler, D., Vermeulen, A. T., Bleeker, A., Erisman, J. W.,  
49 Simpson, D., Zhang, L., Tang, Y. S. and Sutton, M. A.: Dry deposition of reactive nitrogen to  
50 European ecosystems: a comparison of inferential models across the NitroEurope network,  
51 *Atmos. Chem. Phys.*, 11(6), 2703–2728, doi:10.5194/acp-11-2703-2011, 2011.

52 Folberth, G. A., Hauglustaine, D. A., Lathière, J. and Brocheton, F.: Interactive chemistry in the  
53 Laboratoire de Météorologie Dynamique general circulation model: model description and

1 impact analysis of biogenic hydrocarbons on tropospheric chemistry, *Atmos. Chem. Phys.*,  
2 6(8), 2273–2319, doi:10.5194/acp-6-2273-2006, 2006.

3 Fountoukis, C. and Nenes, A.: ISORROPIA II: a computationally efficient thermodynamic  
4 equilibrium model for  $K^+$ - $Ca^{2+}$ - $Mg^{2+}$ - $NH_4^+$ - $Na^+$ - $SO_4^{2-}$ - $NO_3^-$ - $Cl^-$ - $H_2O$  aerosols, *Atmos.*  
5 *Chem. Phys.*, 7(17), 4639–4659, doi:10.5194/acp-7-4639-2007, 2007.

6 Freney, E. J., Sellegri, K., Canonaco, F., Colomb, A., Borbon, A., Michoud, V., Doussin, J.-F.,  
7 Crumeyrolle, S., Amarouche, N., Pichon, J.-M., Bourianne, T., Gomes, L., Prevot, A. S. H.,  
8 Beekmann, M. and Schwarzenböeck, A.: Characterizing the impact of urban emissions on  
9 regional aerosol particles: airborne measurements during the MEGAPOLI experiment, *Atmos.*  
10 *Chem. Phys.*, 14(3), 1397–1412, doi:10.5194/acp-14-1397-2014, 2014.

11 Garcia, L., Bedos, C., Générumont, S., Braud, I. and Cellier, P.: Assessing the ability of mechanistic  
12 volatilization models to simulate soil surface conditions: a study with the Volt’Air model, *Sci.*  
13 *Total Environ.*, 409(19), 3980–92, doi:10.1016/j.scitotenv.2011.05.003, 2011.

14 Générumont, S. and Cellier, P.: A mechanistic model for estimating ammonia volatilization from  
15 slurry applied to bare soil, *Agric. For. Meteorol.*, 88(1-4), 145–167, doi:10.1016/S0168-  
16 1923(97)00044-0, 1997.

17 Gon, H. D. Van Der, Visschedijk, A. and Appelhans, F. J.: A high resolution European emission  
18 data base for the year 2005., 2010.

19 Gong, L., Lewicki, R., Griffin, R. J., Flynn, J. H., Lefer, B. L. and Tittel, F. K.: Atmospheric ammonia  
20 measurements in Houston, TX using an external-cavity quantum cascade laser-based sensor,  
21 *Atmos. Chem. Phys.*, 11(18), 9721–9733, doi:10.5194/acp-11-9721-2011, 2011.

22 Grantz, D. A., Garner, J. H. B. and Johnson, D. W.: Ecological effects of particulate matter.,  
23 *Environ. Int.*, 29(2-3), 213–39, doi:10.1016/S0160-4120(02)00181-2, 2003.

24 Guenther, A., Karl, T., Harley, P., Wiedinmyer, C., Palmer, P. I. and Geron, C.: Estimates of global  
25 terrestrial isoprene emissions using MEGAN (Model of Emissions of Gases and Aerosols from  
26 Nature), *Atmos. Chem. Phys. Discuss.*, 6(1), 107–173, doi:10.5194/acpd-6-107-2006, 2006.

27 Haeffelin, M., Angelini, F., Morille, Y., Martucci, G., Frey, S., Gobbi, G. P., Lolli, S., O’Dowd, C. D.,  
28 Sauvage, L., Xueref-Rémy, I., Wastine, B. and Feist, D. G.: Evaluation of Mixing-Height  
29 Retrievals from Automatic Profiling Lidars and Ceilometers in View of Future Integrated  
30 Networks in Europe, *Boundary-Layer Meteorol.*, 143(1), 49–75, doi:10.1007/s10546-011-  
31 9643-z, 2012.

32 Hamaoui-Laguel, L., Meleux, F., Beekmann, M., Bessagnet, B., Générumont, S., Cellier, P. and  
33 Létinois, L.: Improving ammonia emissions in air quality modelling for France, *Atmos.*  
34 *Environ.*, 92, 584–595, doi:10.1016/j.atmosenv.2012.08.002, 2014.

35 Hansen, M. C., Defries, R. S., Townshend, J. R. G. and Sohlberg, R.: Global land cover  
36 classification at 1 km spatial resolution using a classification tree approach, *Int. J. Remote*  
37 *Sens.*, 21(6-7), 1331–1364, doi:10.1080/014311600210209, 2000.

38 Harrison, R. M. and Pio, C. A.: Size-differentiated composition of inorganic atmospheric  
39 aerosols of both marine and polluted continental origin, *Atmos. Environ.*, 17(9), 1733–1738,  
40 doi:10.1016/0004-6981(83)90180-4, 1983.

41 Hass, H., Van Loon, M., Kessler, C., Stern, R., Matthijsen, J., Sauter, F., Zlatev, Z., Langner, J.,  
42 Foltescu, V. and Schaap, M.: Aerosol modelling: results and intercomparison from European  
43 regional scale modeling systems., 2003.

44 Hauglustaine, D. a.: Interactive chemistry in the Laboratoire de Météorologie Dynamique  
45 general circulation model: Description and background tropospheric chemistry evaluation, *J.*  
46 *Geophys. Res.*, 109(D4), D04314, doi:10.1029/2003JD003957, 2004.

47 Healy, R. M., Sciare, J., Poulain, L., Kamili, K., Merkel, M., Müller, T., Wiedensohler, A., Eckhardt,  
48 S., Stohl, A., Sarda-Estève, R., McGillicuddy, E., O’Connor, I. P., Sodeau, J. R. and Wenger, J. C.:  
49 Sources and mixing state of size-resolved elemental carbon particles in a European megacity:  
50 Paris, *Atmos. Chem. Phys.*, 12(4), 1681–1700, doi:10.5194/acp-12-1681-2012, 2012.

51 IPCC: Climate change 2013 : The physical science basis., 2013.

52 Kanaya, Y., Cao, R., Akimoto, H., Fukuda, M., Komazaki, Y., Yokouchi, Y., Koike, M., Tanimoto, H.,  
53 Takegawa, N. and Kondo, Y.: Urban photochemistry in central Tokyo: 1. Observed and

1 modeled OH and HO<sub>2</sub> radical concentrations during the winter and summer of 2004, *J.*  
2 *Geophys. Res.*, 112(D21312), doi:10.1029/2007JD008670, 2007.

3 Kean, A. J., Littlejohn, D., Ban-Weiss, G. A., Harley, R. A., Kirchstetter, T. W. and Lunden, M. M.:  
4 Trends in on-road vehicle emissions of ammonia, *Atmos. Environ.*, 43(8), 1565–1570,  
5 doi:10.1016/j.atmosenv.2008.09.085, 2009.

6 Kim, Y., Couvidat, F., Sartelet, K. and Seigneur, C.: Comparison of different gas-phase  
7 mechanisms and aerosol modules for simulating particulate matter formation, *J. Air Waste*  
8 *Manage. Assoc.*, 61, 1218–1226, 2011.

9 Konovalov, I. B., Beekmann, M., Richter, a. and Burrows, J. P.: Inverse modelling of the spatial  
10 distribution of NO<sub>x</sub> emissions on a continental scale using satellite data, *Atmos. Chem. Phys.*,  
11 6(7), 1747–1770, doi:10.5194/acp-6-1747-2006, 2006.

12 Kuenen, J. J. P., Visschedijk, A. J. H., Jozwicka, M. and Denier van der Gon, H. A. C.: TNO-MACC\_II  
13 emission inventory; a multi-year (2003–2009) consistent high-resolution European emission  
14 inventory for air quality modelling, *Atmos. Chem. Phys.*, 14(20), 10963–10976,  
15 doi:10.5194/acp-14-10963-2014, 2014.

16 Lombardo, T., Gentaz, L., Verney-Carron, A., Chabas, A., Loisel, C., Neff, D. and Leroy, E.:  
17 Characterisation of complex alteration layers in medieval glasses, *Corros. Sci.*, 72, 10–19,  
18 doi:10.1016/j.corsci.2013.02.004, 2013.

19 Ma, B. L., Wu, T. Y., Tremblay, N., Deen, W., McLaughlin, N. B., Morrison, M. J. and Stewart, G.:  
20 On-Farm Assessment of the Amount and Timing of Nitrogen Fertilizer on Ammonia  
21 Volatilization, *Agron. J.*, 102(1), 134–144, doi:10.2134/agronj2009.0021, 2010.

22 Massad, R.-S., Nemitz, E. and Sutton, M. A.: Review and parameterisation of bi-directional  
23 ammonia exchange between vegetation and the atmosphere, *Atmos. Chem. Phys.*, 10(21),  
24 10359–10386, doi:10.5194/acp-10-10359-2010, 2010.

25 Mather, T. A., Allen, A. G., Davison, B. M., Pyle, D. M., Oppenheimer, C. and McGonigle, A. J. S.:  
26 Nitric acid from volcanoes, *Earth Planet. Sci. Lett.*, 218(1-2), 17–30, doi:10.1016/S0012-  
27 821X(03)00640-X, 2004.

28 Matsumoto, K. and Tanaka, H.: Formation and dissociation of atmospheric particulate nitrate  
29 and chloride: An approach based on phase equilibrium, *Atmos. Environ.*, 30(4), 639–648,  
30 doi:10.1016/1352-2310(95)00290-1, 1996.

31 Menut, L., Bessagnet, B., Khvorostyanov, D., Beekmann, M., Blond, N., Colette, a., Coll, I., Curci,  
32 G., Foret, G., Hodzic, a., Mailler, S., Meleux, F., Monge, J.-L., Pison, I., Siour, G., Turquety, S.,  
33 Valari, M., Vautard, R. and Vivanco, M. G.: CHIMERE 2013: a model for regional atmospheric  
34 composition modelling, *Geosci. Model Dev.*, 6(4), 981–1028, doi:10.5194/gmd-6-981-2013,  
35 2013.

36 Michoud, V., Kukui, A., Camredon, M., Colomb, A., Borbon, A., Miet, K., Aumont, B., Beekmann,  
37 M., Durand-Jolibois, R., Perrier, S., Zapf, P., Siour, G., Ait-Helal, W., Locoge, N., Sauvage, S., Afif,  
38 C., Gros, V., Furger, M., Ancellet, G. and Doussin, J. F.: Radical budget analysis in a suburban  
39 European site during the MEGAPOLI summer field campaign, *Atmos. Chem. Phys.*, 12(24),  
40 11951–11974, doi:10.5194/acp-12-11951-2012, 2012.

41 Moya, M., Ansari, A. S. and Pandis, S. N.: Partitioning of nitrate and ammonium between the  
42 gas and particulate phases during the 1997 IMADA-AVER study in Mexico City, *Atmos.*  
43 *Environ.*, 35(10), 1791–1804, doi:10.1016/S1352-2310(00)00292-2, 2001.

44 Mozurkewich, M.: The dissociation constant of ammonium nitrate and its dependence on  
45 temperature, relative humidity and particle size, *Atmos. Environ. Part A. Gen. Top.*, 27(2),  
46 261–270, doi:10.1016/0960-1686(93)90356-4, 1993.

47 Mulawa, P. A., Cadle, S. H., Lipari, F., Ang, C. C. and Vandervennet, R.: Urban dew: Its  
48 composition and influence on dry deposition rates, *Atmos. Environ.*, 20(7), 1389–1396,  
49 doi:10.1016/0004-6981(86)90009-0, 1986.

50 Nenes, A., Pandis, S. and Pilinis, C.: ISORROPIA : A New Thermodynamic Equilibrium Model for  
51 Multiphase Multicomponent Inorganic Aerosols, *Aquat. geochemistry*, 4(1), 123–152, 1998.

52 Nenes, A., Pandis, S. N. and Pilinis, C.: Continued development and testing of a new  
53 thermodynamic aerosol module for urban and regional air quality models, *Atmos. Environ.*,

1 33(10), 1553–1560, doi:10.1016/S1352-2310(98)00352-5, 1999.  
2 Neuman, J. A., Huey, L. G., Ryerson, T. B. and Fahey, D. W.: Study of inlet materials for sampling  
3 atmospheric nitric acid, *Environ. Sci. Technol.*, 33(7), 1133–1136, doi:10.1021/es980767f,  
4 1999.  
5 Norman, M., Spirig, C., Wolff, V., Trebs, I., Flechard, C., Wisthaler, A., Schnitzhofer, R., Hansel, A.  
6 and Neftel, A.: Intercomparison of ammonia measurement techniques at an intensively  
7 managed grassland site (Oensingen, Switzerland), *Atmos. Chem. Phys.*, 9(8), 2635–2645,  
8 doi:10.5194/acp-9-2635-2009, 2009.  
9 Ottley, C. J. and Harrison, R. M.: The spatial distribution and particle size of some inorganic  
10 nitrogen, sulphur and chlorine species over the North Sea, *Atmos. Environ. Part A. Gen. Top.*,  
11 26(9), 1689–1699, doi:10.1016/0960-1686(92)90067-U, 1992.  
12 Pang, Y., Eatough, N. L., Wilson, J. and Eatough, D. J.: Effect of Semivolatile Material on PM<sub>2.5</sub>  
13 Measurement by the PM<sub>2.5</sub> Federal Reference Method Sampler at Bakersfield, California,  
14 *Aerosol Sci. Technol.*, 36(3), 289–299, doi:10.1080/027868202753504489, 2002.  
15 Parmar, R. ., Satsangi, G. ., Lakhani, A., Srivastava, S. . and Prakash, S.: Simultaneous  
16 measurements of ammonia and nitric acid in ambient air at Agra (27°10'N and 78°05'E)  
17 (India), *Atmos. Environ.*, 35(34), 5979–5988, doi:10.1016/S1352-2310(00)00394-0, 2001.  
18 Pay, M. T., Jiménez-Guerrero, P. and Baldasano, J. M.: Assessing sensitivity regimes of  
19 secondary inorganic aerosol formation in Europe with the CALIOPE-EU modeling system,  
20 *Atmos. Environ.*, 51, 146–164, doi:10.1016/j.atmosenv.2012.01.027, 2012.  
21 Perrino, C., Catrambone, M., Di Menno Di Bucchianico, A. and Allegrini, I.: Gaseous ammonia in  
22 the urban area of Rome, Italy and its relationship with traffic emissions, *Atmos. Environ.*,  
23 36(34), 5385–5394, doi:10.1016/S1352-2310(02)00469-7, 2002.  
24 Petetin, H., Beekmann, M., Sciare, J., Bressi, M., Rosso, A., Sanchez, O. and Gherzi, V.: A novel  
25 model evaluation approach focusing on local and advected contributions to urban PM<sub>2.5</sub>  
26 levels – application to Paris, France, *Geosci. Model Dev.*, 7(4), 1483–1505, doi:10.5194/gmd-  
27 7-1483-2014, 2014.  
28 Petit, J.-E., Favez, O., Sciare, J., Crenn, V., Sarda-Estève, R., Bonnaire, N., Močnik, G., Dupont, J.-C.,  
29 Haefelin, M. and Leoz-Garziandia, E.: Two years of near real-time chemical composition of  
30 submicron aerosols in the region of Paris using an Aerosol Chemical Speciation Monitor  
31 (ACSM) and a multi-wavelength Aethalometer, *Atmos. Chem. Phys.*, 15(6), 2985–3005,  
32 doi:10.5194/acp-15-2985-2015, 2015.  
33 Pierson, W. R., Brachaczek, W. W., Japar, S. M., Cass, G. R. and Solomon, P. A.: Dry deposition  
34 and dew chemistry in Claremont, California, during the 1985 nitrogen species methods  
35 comparison study, *Atmos. Environ.*, 22(8), 1657–1663, doi:10.1016/0004-6981(88)90393-9,  
36 1988.  
37 Platt, U., Perner, D., Schröder, J., Kessler, C. and Toenissen, A.: The diurnal variation of NO<sub>3</sub>, J.  
38 *Geophys. Res.*, 86, 11965–11970, 1981.  
39 Pleim, J. E., Bash, J. O., Walker, J. T. and Cooter, E. J.: Development and evaluation of an  
40 ammonia bidirectional flux parameterization for air quality models, *J. Geophys. Res. Atmos.*,  
41 118(9), 3794–3806, doi:10.1002/jgrd.50262, 2013.  
42 Pope, C. A., Ezzati, M. and Dockery, D. W.: Fine-particulate air pollution and life expectancy in  
43 the United States., *N. Engl. J. Med.*, 360(4), 376–86, doi:10.1056/NEJMsa0805646, 2009.  
44 Pouliot, G., Pierce, T., Denier van der Gon, H., Schaap, M., Moran, M. and Nopmongkol, U.:  
45 Comparing emission inventories and model-ready emission datasets between Europe and  
46 North America for the AQMEII project, *Atmos. Environ.*, 53, 4–14,  
47 doi:10.1016/j.atmosenv.2011.12.041, 2012.  
48 Putaud, J.-P., Van Dingenen, R., Alastuey, A., Bauer, H., Birmili, W., Cyrus, J., Flentje, H., Fuzzi, S.,  
49 Gehrig, R., Hansson, H. C., Harrison, R. M., Herrmann, H., Hitzenberger, R., Hüglin, C., Jones, A.  
50 M., Kasper-Giebl, A., Kiss, G., Kousa, A., Kuhlbusch, T. a. J., Löschan, G., Maenhaut, W., Molnar,  
51 A., Moreno, T., Pekkanen, J., Perrino, C., Pitz, M., Puxbaum, H., Querol, X., Rodriguez, S., Salma, I.,  
52 Schwarz, J., Smolik, J., Schneider, J., Spindler, G., ten Brink, H., Tursic, J., Viana, M.,  
53 Wiedensohler, A. and Raes, F.: A European aerosol phenomenology - 3 : Physical and chemical

1 characteristics of particulate matter from 60 rural, urban, and kerbside sites across Europe,  
2 *Atmos. Environ.*, 44(10), 1308–1320, doi:10.1016/j.atmosenv.2009.12.011, 2010.

3 Reche, C., Viana, M., Pandolfi, M., Alastuey, A., Moreno, T., Amato, F., Ripoll, A. and Querol, X.:  
4 Urban NH<sub>3</sub> levels and sources in a Mediterranean environment, *Atmos. Environ.*, 57, 153–164,  
5 doi:10.1016/j.atmosenv.2012.04.021, 2012.

6 Sartelet, K., Debry, E., Fahey, K., Roustan, Y., Tombette, M. and Sportisse, B.: Simulation of  
7 aerosols and gas-phase species over Europe with the Polyphemus system: Part I - Model-to-  
8 data comparison for 2001, *Atmos. Environ.*, 41(29), 6116–6131,  
9 doi:10.1016/j.atmosenv.2007.04.024, 2007.

10 Schaap, M., Timmermans, R. M. A., Roemer, M., Boersen, G. A. C., Bultjes, P. J. H., Sauter, F. J.,  
11 Velders, G. J. M. and Beck, J. P.: The LOTOS EUROS model: description, validation and latest  
12 developments, *Int. J. Environ. Pollut.*, 32(2), 270, doi:10.1504/IJEP.2008.017106, 2008.

13 Schmidt, H. and Derognat, C.: A comparison of simulated and observed ozone mixing ratios for  
14 the summer of 1998 in Western Europe, *Atmos. Environ.*, 35, 6277–6297, 2001.

15 Sciare, J., d'Argouges, O., Zhang, Q. J., Sarda-Estève, R., Gaimoz, C., Gros, V., Beekmann, M. and  
16 Sanchez, O.: Comparison between simulated and observed chemical composition of fine  
17 aerosols in Paris (France) during springtime: contribution of regional versus continental  
18 emissions, *Atmos. Chem. Phys.*, 10(24), 11987–12004, doi:10.5194/acp-10-11987-2010,  
19 2010.

20 Sciare, J., D'Argouges, O., Sarda-Estève, R., Gaimoz, C., Dolgorouky, C., Bonnaire, N., Favez, O.,  
21 Bonsang, B. and Gros, V.: Large contribution of water-insoluble secondary organic aerosols in  
22 the region of Paris (France) during wintertime, *J. Geophys. Res.*, 116(D22203),  
23 doi:10.1029/2011JD015756, 2011.

24 Seinfeld, J. H. and Pandis, S. N.: *Atmospheric Chemistry and Physics: From Air Pollution to*  
25 *Climate Change*, John Wiley, New York., 2006.

26 Skjøth, C. A., Geels, C., Berge, H., Gyldenkerne, S., Fagerli, H., Ellermann, T., Frohn, L. M.,  
27 Christensen, J., Hansen, K. M., Hansen, K. and Hertel, O.: Spatial and temporal variations in  
28 ammonia emissions – a freely accessible model code for Europe, *Atmos. Chem. Phys.*, 11(11),  
29 5221–5236, doi:10.5194/acp-11-5221-2011, 2011.

30 Solomon, P. A., Salmon, L. G., Fall, T. and Cass, G. R.: Spatial and temporal distribution of  
31 atmospheric nitric acid and particulate nitrate concentrations in the Los Angeles area,  
32 *Environ. Sci. Technol.*, 26(8), 1594–1601, doi:10.1021/es00032a016, 1992.

33 Stern, R.: *Entwicklung und Anwendung des chemischen Transportmodells REM/CALGRID.*  
34 *Berichte zum UBA Forschungsvorhaben 298 41 252*, Freie Universität Berlin, Institut für  
35 Meteorologie., 2003.

36 Stohl, A., Haimberger, L., Scheele, M. P. and Wernli, H.: An intercomparison of results from  
37 three trajectory models, *Meteorol. Appl.*, 8(2), 127–135, doi:10.1017/S1350482701002018,  
38 2001.

39 Sutton, M. ., Dragosits, U., Tang, Y. . and Fowler, D.: Ammonia emissions from non-agricultural  
40 sources in the UK, *Atmos. Environ.*, 34(6), 855–869, doi:10.1016/S1352-2310(99)00362-3,  
41 2000.

42 Takahama, S., Wittig, A. E., Vayenas, D. V., Davidson, C. I. and Pandis, S. N.: Modeling the diurnal  
43 variation of nitrate during the Pittsburgh Air Quality Study, *J. Geophys. Res.*, 109(D16),  
44 D16S06, doi:10.1029/2003JD004149, 2004.

45 Trebs, I., Meixner, F. X., Slanina, J., Otjes, R., Jongejan, P. and Andreae, M. O.: Real-time  
46 measurements of ammonia, acidic trace gases and water-soluble inorganic aerosol species at a  
47 rural site in the Amazon Basin, *Atmos. Chem. Phys.*, 4(4), 967–987, doi:10.5194/acp-4-967-  
48 2004, 2004.

49 Trebs, I., Andreae, M. O., Elbert, W., Mayol-Bracero, O. L., Soto-García, L. L., Rudich, Y.,  
50 Falkovich, A. H., Maenhaut, W., Artaxo, P., Otjes, R. and Slanina, J.: Aerosol inorganic  
51 composition at a tropical site: discrepancies between filter-based sampling and a semi-  
52 continuous method, *Aerosol Sci. Technol.*, 42(4), 255–269,  
53 doi:10.1080/02786820801992899, 2008.



1 Vayenas, D. V., Takahama, S., Davidson, C. I. and Pandis, S. N.: Simulation of the  
2 thermodynamics and removal processes in the sulfate-ammonia-nitric acid system during  
3 winter: Implications for PM<sub>2.5</sub> control strategies, *J. Geophys. Res.*, 110(D7), D07S14,  
4 doi:10.1029/2004JD005038, 2005.

5 Vrekoussis, M., Kanakidou, M., Mihalopoulos, N., Crutzen, P. J., Lelieveld, J., Perner, D.,  
6 Berresheim, H. and Baboukas, E.: Role of the NO<sub>3</sub> radicals in oxidation processes in the  
7 eastern Mediterranean troposphere during the MINOS campaign, *Atmos. Chem. Phys.*, 4(1),  
8 169–182, doi:10.5194/acp-4-169-2004, 2004.

9 Wesely, M. L.: Parameterization of surface resistances to gaseous dry deposition in regional-  
10 scale numerical models, *Atmos. Environ.*, 23(6), 1293–1304, doi:10.1016/0004-  
11 6981(89)90153-4, 1989.

12 Wichink Kruit, R. J. (Roy), van Pul, W. A. J., Otjes, R. P., Hofschreuder, P., Jacobs, A. F. G. and  
13 Holtslag, A. A. M.: Ammonia fluxes and derived canopy compensation points over non-  
14 fertilized agricultural grassland in The Netherlands using the new gradient ammonia—high  
15 accuracy—monitor (GRAHAM), *Atmos. Environ.*, 41(6), 1275–1287,  
16 doi:10.1016/j.atmosenv.2006.09.039, 2007.

17 Yao, X., Hu, Q., Zhang, L., Evans, G. J., Godri, K. J. and Ng, A. C.: Is vehicular emission a significant  
18 contributor to ammonia in the urban atmosphere?, *Atmos. Environ.*, 80, 499–506,  
19 doi:10.1016/j.atmosenv.2013.08.028, 2013.

20 Yin, J. and Harrison, R. M.: Pragmatic mass closure study for PM<sub>1.0</sub>, PM<sub>2.5</sub> and PM<sub>10</sub> at  
21 roadside, urban background and rural sites, *Atmos. Environ.*, 42(5), 980–988,  
22 doi:10.1016/j.atmosenv.2007.10.005, 2008.

23 Zhang, L., Wright, L. P. and Asman, W. A. H.: Bi-directional air-surface exchange of atmospheric  
24 ammonia: A review of measurements and a development of a big-leaf model for applications  
25 in regional-scale air-quality models, *J. Geophys. Res.*, 115(D20310), 1–23,  
26 doi:10.1029/2009JD013589, 2010.

27